Article

# Discovery of the Soluble Guanylate Cyclase Stimulator Vericiguat (BAY 1021189) for the Treatment of Chronic Heart Failure

Markus Follmann, Jens Ackerstaff, Gorden Redlich, Frank Wunder, Dieter Lang, Armin Kern, Peter Fey, Nils Griebenow, Walter Kroh, Eva-Maria Becker-Pelster, Axel Kretschmer, Volker Geiss, Volkhart Li, Alexander Straub, Joachim Mittendorf, Rolf Jautelat, Hartmut Schirok, Karl-Heinz Schlemmer, Klemens Lustig, Michael Gerisch, Andreas Knorr, Hanna Tinel, Thomas Mondritzki, Hubert Trübel, Peter Sandner, and Johannes-Peter Stasch

*J. Med. Chem.*, **Just Accepted Manuscript** • Publication Date (Web): 30 May 2017

# Discovery of the Soluble Guanylate Cyclase Stimulator Vericiguat (BAY 1021189) for the Treatment of Chronic Heart Failure

*Markus Follmann,* Jens Ackerstaff, Gorden Redlich, Frank Wunder, Dieter Lang, Armin Kern, Peter Fey, Nils Griebenow, Walter Kroh, Eva-Maria Becker-Pelster, Axel Kretschmer, Volker Geiss, Volkhart Li, Alexander Straub, Joachim Mittendorf, Rolf Jautelat, Hartmut Schirok, Karl-Heinz Schlemmer, Klemens Lustig, Michael Gerisch, Andreas Knorr, Hanna Tinel, Thomas Mondritzki, Hubert Trübel, Peter Sandner, and Johannes-Peter Stasch*

Bayer AG, Drug Discovery, Aprather Weg 18a, 42113 Wuppertal, Germany

**ABSTRACT:** The first-in-class soluble guanylate cyclase (sGC) stimulator riociguat was recently introduced as a novel treatment option for pulmonary hypertension. Despite its outstanding pharmacological profile, application of riociguat in other cardiovascular indications is limited by its short half-life, necessitating a three times daily dosing regimen. In our efforts to further optimize the compound class, we have uncovered interesting structure–activity relationships and were able to decrease oxidative metabolism significantly. These studies resulting in the discovery of once daily sGC stimulator vericiguat (compound **24**, BAY 1021189), currently in phase 3 trials for chronic heart failure, are now reported.

## INTRODUCTION

The NO–sGC–cGMP axis belongs to the key signal transduction pathways involved in regulating the cardiovascular system.[1, 2] Central to this pathway is soluble guanylate cyclase (sGC), an intracellular enzyme present in the smooth muscle cells of blood vessels and in platelets but also in various other cell types like cardiomyocytes. sGC displays a high affinity for, and is activated by, the first messenger signaling molecule nitric oxide (NO). Biosynthesis of NO is mediated by three distinct isoforms of nitric oxide synthases, endothelial nitric oxide synthase (eNOS), neuronal nitric oxide synthase (nNOS) and the inducible isoform of nitric oxide synthase (iNOS), all synthesizing NO from L-arginine. Within endothelial cells, NO is produced by eNOS and diffuses rapidly to the underlying smooth muscle cells where it binds to its target enzyme sGC. This binding leads to the stimulation of sGC resulting in increased production of intracellular second messenger cGMP. cGMP interacts with three types of intracellular proteins such as cGMP-dependent protein kinases, cGMP-regulated ion channels and phosphodiesterases. Further downstream, these transduction cascades mediate various physiological and tissue-protective effects including smooth muscle relaxation and inhibition of smooth muscle proliferation, leukocyte recruitment and platelet function. The pathogenesis of various diseases, especially those of the cardiovascular system, has been related to insufficient bioavailability of NO and thus impaired stimulation of sGC and therefore decreased cGMP production.[3-7]

sGC itself is a cytosolic, heterodimeric protein composed of an α- and a β-subunit with a prosthetic heme group located in the β-subunit (heme-binding domain).[8-13] Mechanistically, NO stimulates sGC by binding to the $Fe^{2+}$ of the heme group, which induces cleavage of an $Fe^{2+}$–

histidine ($His^{105}$) bond, likely resulting in conformational reorganizations which propagate into the catalytic subunit, increasing cGMP production. cGMP interacts with three types of intracellular proteins, namely cGMP-dependent protein kinases, cGMP-regulated ion channels and phosphodiesterases. Further downstream, these transduction cascades mediate various physiological and tissue-protective effects, including smooth muscle relaxation and inhibition of smooth muscle proliferation, leukocyte recruitment and platelet function.[1]

sGC can exist in two different states, a native heme-containing or reduced form of sGC, which is the endogenous receptor for NO, and a heme-free form of sGC.[1, 14] Under conditions of oxidative stress, which is thought to be causal in the pathogenesis of many cardiovascular diseases, reactive oxygen species (ROS) are produced. ROS are capable of oxidizing the heme iron of sGC ($Fe^{2+} \rightarrow Fe^{3+}$), resulting ultimately in heme loss from oxidized sGC. As a consequence, the heme-free form of sGC is no longer binding NO, is not responsive to NO and thus termed dysfunctional. During the last 20 years, two distinct compound classes have been discovered at Bayer that are capable of activating sGC in a NO-independent manner, the heme-dependent sGC stimulators and the heme-independent sGC activators. sGC stimulators display a dual mode of action: they synergize with endogenous NO and, on top of this, are also able to directly stimulate the native form of the enzyme independently of NO, resulting in increased cGMP production.[15] In contrast, sGC activators are capable of activating the dysfunctional heme-free sGC, resulting in increased cGMP production even under conditions of reduced NO bioavailability.[16]

The discovery of the sGC stimulators at Bayer, along with the efforts of several other pharmaceutical companies to identify sGC stimulators and activators, has recently been reviewed.[2] Riociguat (**1**) is the first sGC stimulator to have made a successful transition from animal experiments to controlled clinical studies in patients.[17] In 2013 **1** gained market approval

for two life-threatening diseases: pulmonary arterial hypertension (PAH)[18] and chronic thromboembolic pulmonary hypertension (CTEPH).[19, 20] However, application of **1** in other cardiovascular indications, such as heart failure, is limited by its short half-life.[21]

Herein, we report our recent efforts in optimizing the pharmacokinetic profile of sGC stimulators, culminating in the discovery of vericiguat (compound **24**, BAY 1021189), which has been evaluated in phase 2 studies (SOCRATES trials) in heart failure patients with reduced (HFrEF) and preserved (HFpEF) ejection fraction.[22, 23] Currently, **24** is being investigated in a phase 3 outcome study (VICTORIA trial) in heart failure patients with HFrEF in co-development with MSD (vericiguat code name: MK-1242).[24] That study is aimed at assessing whether **24**, on top of standard of care, is able to decrease mortality and morbidity in such HFrEF patients.

## RESULTS AND DISCUSSION

**Optimization Strategy.** Our goal was to identify orally bioavailable sGC stimulators with a longer duration of action than **1**, in order to support a profile allowing for a once daily oral dosing, and less oxidative metabolism in order to lower interaction potentials. **1** is a very potent sGC stimulator in vitro and in vivo; however, it has a moderate half-life in different animal species[25] and this pharmacokinetic profile translated into a three times daily dosing regimen in patients. *N*-demethylation to compound **9**, as described by Gnoth et al.[26] in 2015, is the major biotransformation of **1** and is mainly catalyzed by CYP1A1, and also by CYP3A4, CYP3A5 and CYP2J2.[21, 26-31] Our strategy was to further optimize the metabolic stability of **1** and hence reduce blood clearance to achieve a longer half-life. We began by optimizing the substituents on the 5-carbamoyl residue on the pyrimidine ring, aiming to achieve metabolically more stable

derivatives while maintaining good potency. Later, in a second optimization step, we focused on variations of the central pyrazolopyridine scaffold.

**Chemistry.** Scheme 1 outlines the strategy for the synthesis of the 5-carbamoyl variations. Starting from triamine **1c**, which is available in two steps from amidine **1a** and phenyldiazenyl-substituted malonodinitrile **1b**, selective carbamate formation at the 5-amino group was achieved either by treatment with the corresponding chloroformate or by addition of the respective alcohol preactivated with triphosgene, to yield compounds **9**–**14**.[25] Deprotonation of the carbamate NH group and subsequent treatment with the corresponding halide or trichloromethanesulfonate electrophile allowed further derivatization to the corresponding N-alkylated carbamates (**1**, **2**, **4**–**8**). Alternatively, the alkyl side chain on the 5-amino group could first be introduced via reductive amination and the product **1d** subsequently treated with methyl chloroformate, giving access to the hydroxyethyl derivative **3**. For the cyclic 5-(2-oxo-1,3-oxazolidin-3-yl) analogues **15**–**18**, the previously employed conditions for the selective formation of carbamates provided **1e**–**g** bearing a chloro- or bromo-substituted alkyl chain, allowing for a base-induced intramolecular cyclization (NaHMDS).

**Scheme 1.** Synthesis of Compounds **1**–**18**[a]

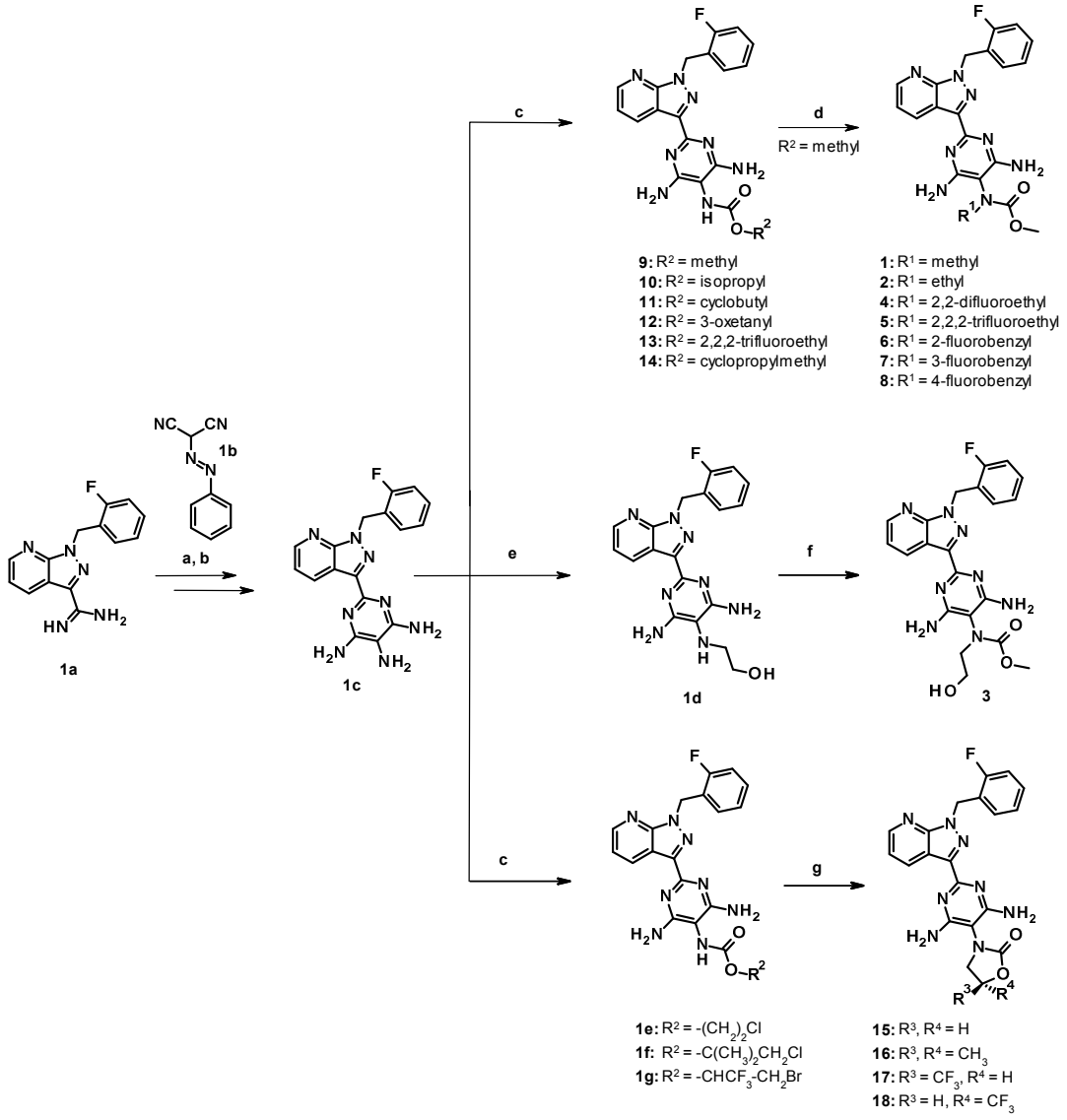


[a]Reagents and conditions: (a) NaOMe, DMF, 110 °C. (b) $H_2$ (65 bar), Raney nickel, DMF. (c) $R^2OCOCl$, pyridine, or i. triphosgene, pyridine, ii. $R^2OH$, pyridine. (d) $R^1X$ (X = halide or trichloromethanesulfonate), LiHMDS. (e) glycolaldehyde, $NaBH_3CN$, AcOH, MeOH, 0 °C to rt. (f) methyl chloroformate, pyridine, rt. (g) NaHMDS, THF, 0 °C to rt.

The synthesis of the compounds with a core variation is outlined in Schemes 2–5. For the 1*H*-pyrazolo[4,3-*b*]pyridine derivative **19**, the synthesis started from 3,5-dichloropyridine-2-carbonyl chloride (**2a**) which was converted into 3-(2-fluorobenzyl)-1*H*-pyrazolo[4,3-*b*]pyridine (**2b**) in four steps. The fluoro derivative **2d** was synthesized in a similar manner from the corresponding difluoropyridine analogue **2c**. Both key intermediates **2b** and **2d** were then reacted with 2-chloro-

5-nitropyrimidine-4,6-diamine,[32] followed by reduction of the pyrimidine 5-nitro group and methyl carbamate formation, to give the 1*H*-pyrazolo[4,3-*b*]pyridine core analogues **19** and **20** (Scheme 2).

**Scheme 2.** Synthesis of Compounds **19** and **20**[a]

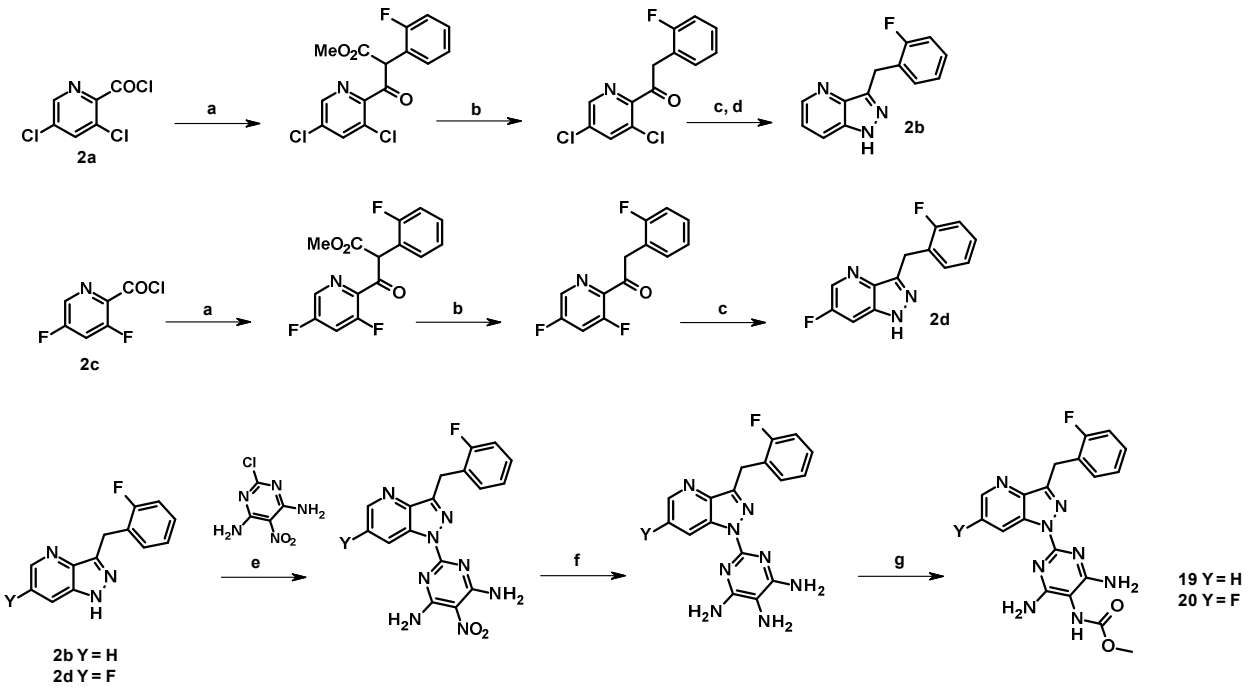


[a]Reagents and conditions: (a) methyl 2-(2-fluorophenyl)acetate, LiHMDS. (b) aq NaCl solution, DMSO, microwave, 150 °C. (c) hydrazine hydrate, pyridine, reflux. (d) $H_2$, 10% Pd/C, $Et_3N$, EtOH, THF. (e) NaH, DMF, 80 °C. (f) $H_2$, 10% Pd/C, pyridine. (g) methyl chloroformate, pyridine.

A different route was used for the preparation of 1*H*-pyrazolo[3,4-*c*]pyridazine **21** (Scheme 3), which began with the cyclization of methyl 2-aminothiophene-3-carboxylate (**3a**) with hydrazine hydrate to give 1*H*-pyrazolo[3,4-*c*]pyridazin-3-ol (**3b**).[33] Subsequent bromination afforded intermediate **3c** which was alkylated with 2-fluorobenzyl bromide to yield **3d**. Then, conversion of the bromide into the cyanide **3e** and Pinner-type reaction of the cyano group with sodium methoxide and ammonium chloride afforded key intermediate **3f**. Further modifications,

analogous to the formation of carbamate **9** from **1a** (Scheme 1), yielded the methyl carbamate derivative **21**.

**Scheme 3.** Synthesis of Compound **21**[a]

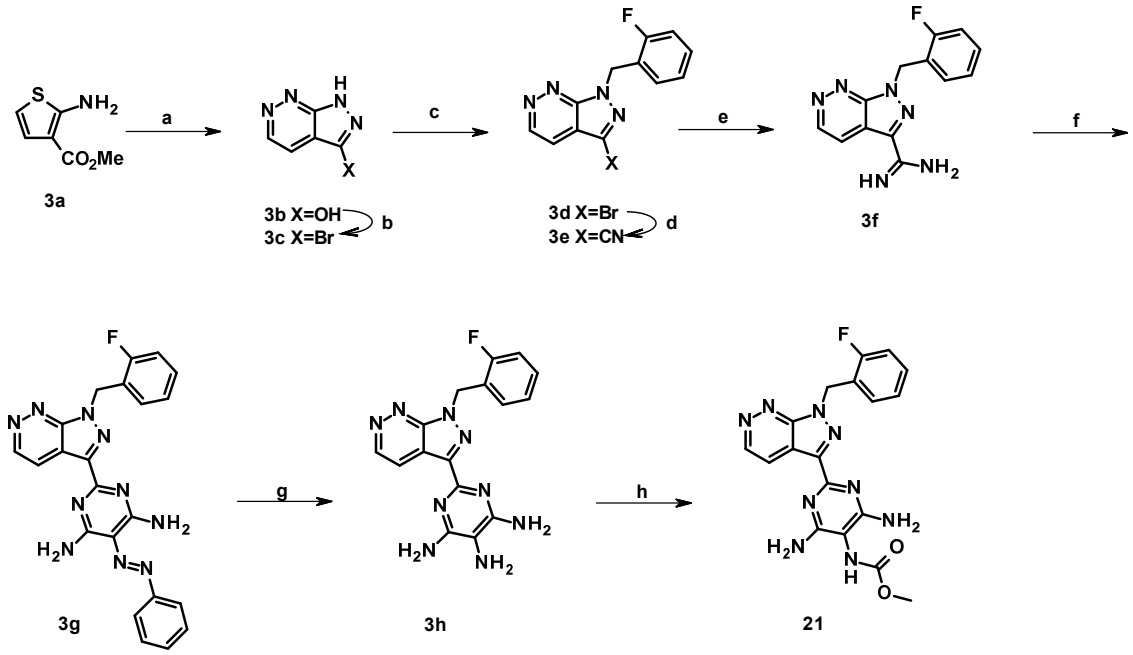


[a]Reagents and conditions: (a) hydrazine hydrate. (b) $POBr_3$, sulfolane, 150 °C. (c) 2-fluorobenzyl bromide, $Cs_2CO_3$, DMF, rt. (d) CuCN, DMSO, 150 °C. (e) NaOMe, $NH_4Cl$, AcOH, MeOH. (f) **1b**, DMF, $Et_3N$, 100 °C. (g) $H_2$ (1 bar), 10% Pd/C, DMF. (h) methyl chloroformate, pyridine, DCM.

The preparation of imidazo[1,5-*a*]pyrimidine **22** (Scheme 4) started with condensation of the readily available thioimide **4a** and amine **4b** to access aminoimidazole **4c**. Further orthoester condensation then gave the bicyclic imidazopyrimidine derivative **4d** bearing an ethyl ester functionality. Subsequent saponification, amidation and dehydration yielded nitrile **4g** as a key intermediate. Pinner-type reaction with sodium methoxide and ammonium chloride delivered the corresponding amidine **4h** which could be converted into the final compound **22** in analogy to the previous examples.

**Scheme 4.** Synthesis of Compound **22**[a]

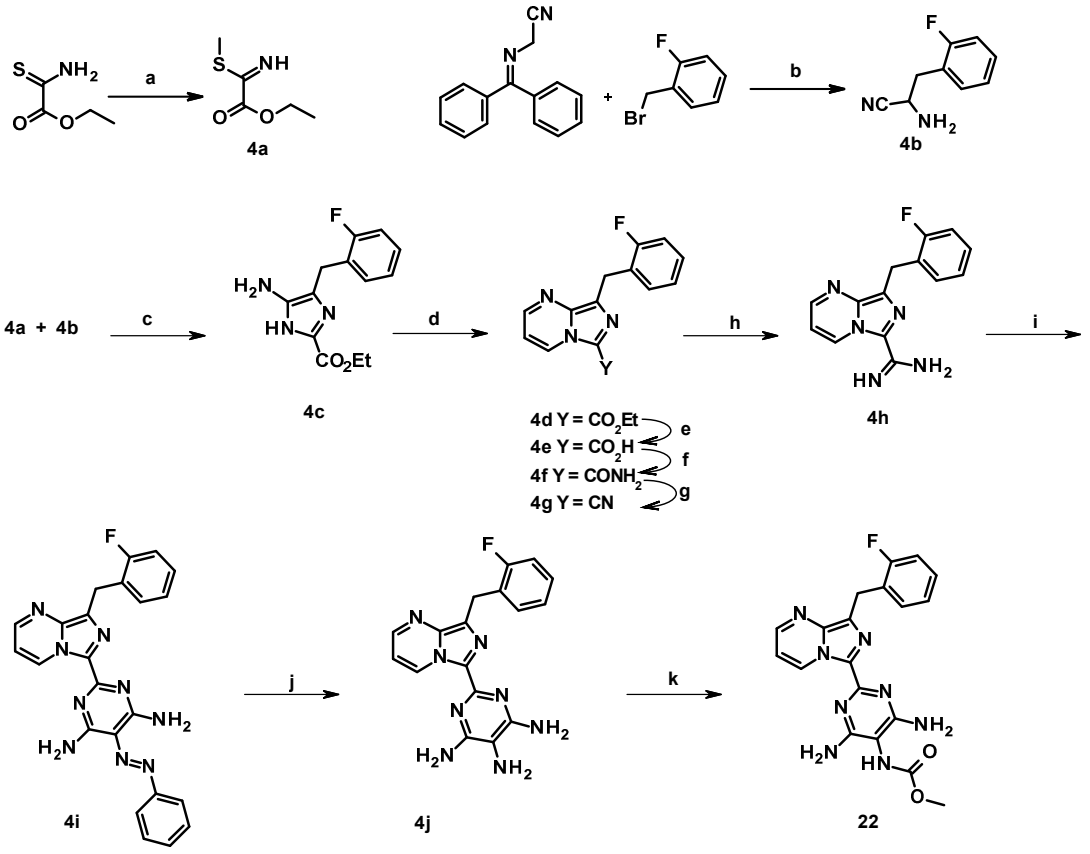


[a]Reagents and conditions: (a) MeI, $K_2CO_3$, acetone. (b) TBAI, KO*t*-Bu, DCM, then aq HCl, $Et_2O$. (c) dioxane, 60 °C. (d) 1,1,3,3-tetramethoxypropane, aq HCl, MeOH, EtOH, reflux. (e) NaOH. (f) HATU, $NH_4Cl$, Hünig's base, DMF. (g) $POCl_3$, 120 °C. (h) NaOMe, $NH_4Cl$, MeOH. (i) **1b**, DMF, $Et_3N$, 100 °C. (j) $H_2$ (1 bar), 10% Pd/C, DMF, 0 °C. (k) methyl chloroformate, pyridine.

The synthesis of the related imidazo[1,5-*b*]pyridazine derivative **23** (Scheme 5) started from methyl 5-aminolevulinate hydrochloride (**5a**). Addition of hydrazine hydrate yielded the dihydropyridazinone **5b** which was reacted with the readily available acid chloride **5c** under basic conditions. The resulting amide was oxidized with bromine to provide the corresponding pyridazinone **5d** which underwent an intramolecular condensation in the presence of phosphoryl chloride to give the bicyclic intermediate **5e**. Dechlorination of the pyridazine core catalyzed by palladium on charcoal and subsequent bromination of the imidazo core with *N*-

bromosuccinimide gave access to **5f**. Further modifications, as outlined previously, then yielded amidine **5g** as a key intermediate which was converted into the final target compound **23**.

**Scheme 5.** Synthesis of Compound **23**[a]

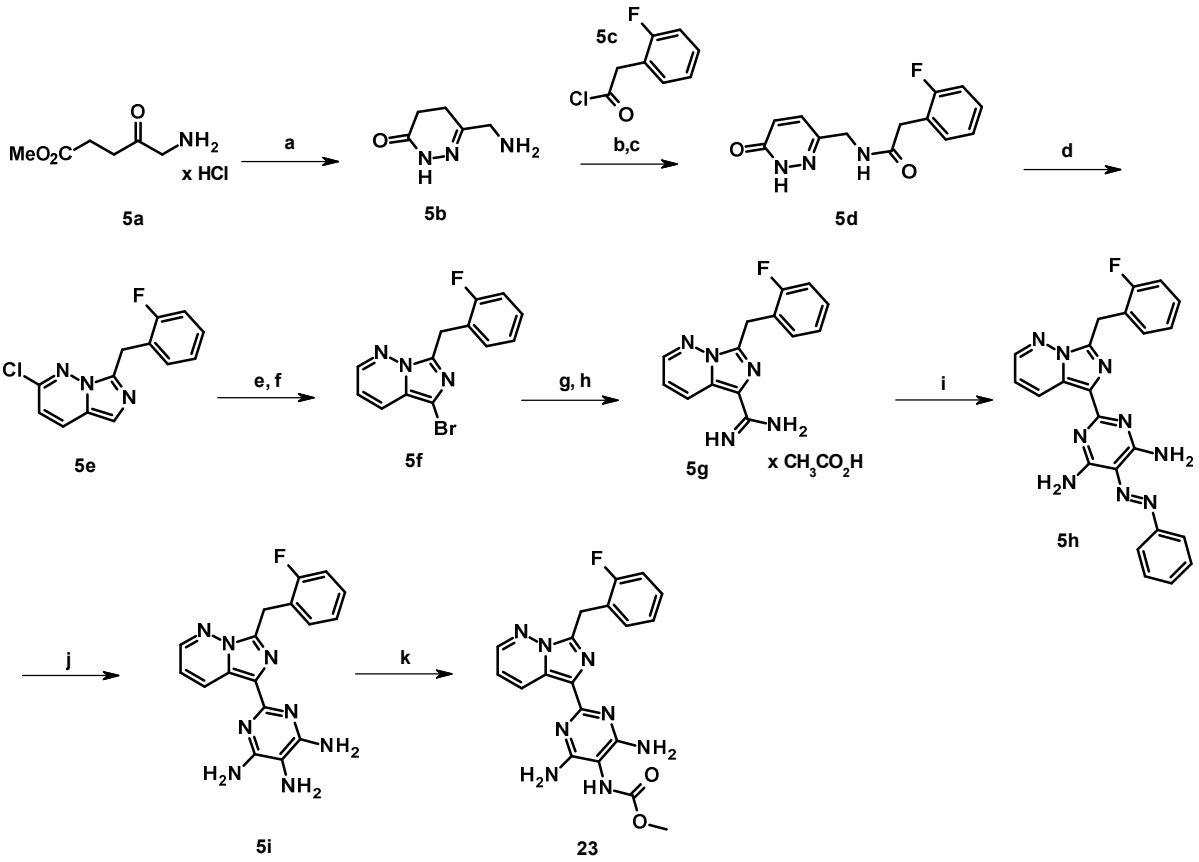


[a]Reagents and conditions: (a) hydrazine hydrate, $Et_3N$, reflux. (b) $Et_3N$, MeCN. (c) $Br_2$, AcOH, 50 °C. (d) $POCl_3$, DCE, reflux. (e) $H_2$, 5% Pd/C, $Et_3N$, EtOAc. (f) NBS, DCM. (g) CuCN. (h) NaOMe, $NH_4Cl$, AcOH. (i) **1b**, DMF, $Et_3N$, 100 °C. (j) $H_2$ (1 bar), 10% Pd/C, DMF, MeOH. (k) methyl chloroformate, pyridine.

The synthesis of the 1*H*-pyrazolo[3,4-*b*]pyridine derivative (**24)** (Scheme 6), involved initial activation of 2,2,3,3-tetrafluoro-1-propanol (**6a**) with trifluoromethanesulfonic anhydride and treatment with morpholine to yield **6b** after aqueous workup and distillation. At 135 °C, **6b** was alkylated with methyl methanesulfonate leading to quaternized derivative **6c** which was converted into **6d** using sodium hydroxide. Further reaction with morpholine and triethylamine

yielded **6e** after crystallization from toluene. Acrylaldehyde derivative **6e** was reacted with ethyl 5-amino-1-(2-fluorobenzyl)-1*H*-pyrazole-3-carboxylate[25] in ethanol yielding ethyl ester intermediate **6f**. Ester **6f** was then converted in three steps into the corresponding amidine **6i** via amide **6g** and nitrile **6h** in analogy to the chemistry outlined in Scheme 4. The synthesis of **24** was completed as described for compound **9** (Scheme 1) via the diazenyl derivative **6j** and triamine **6k**.

**Scheme 6.** Synthesis of **24**[a]

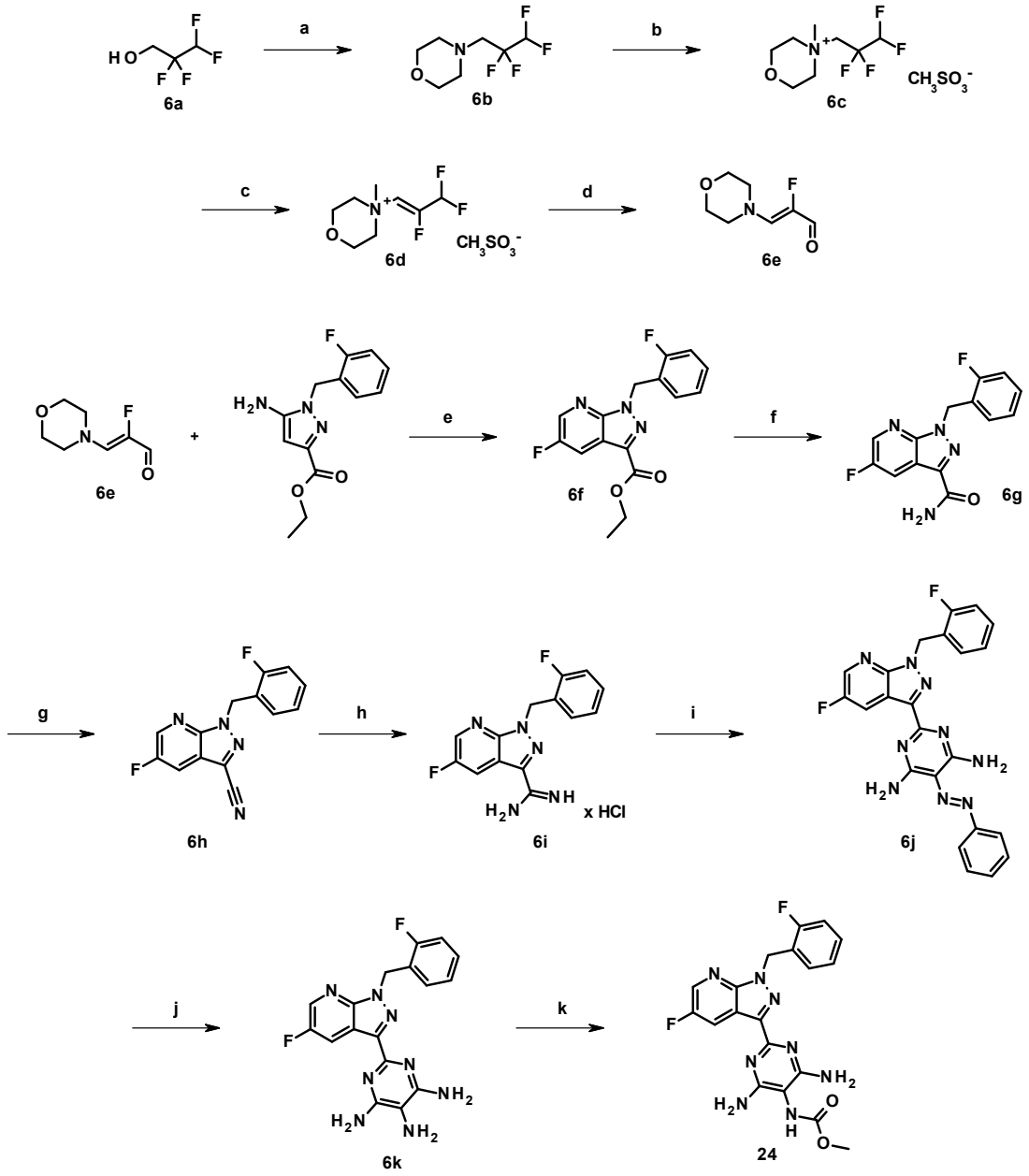


[a]Reagents and conditions: (a) $Tf_2O$, 70 °C, then morpholine, 5 °C, then 40 °C. (b) $MeSO_3Me$, 135 °C, then 100 °C. (c) 45% aq NaOH, 50 °C. (d) morpholine, $Et_3N$, reflux. (e) MsOH, LiCl, EtOH, reflux. (f) formamide, NaOMe, MeOH, EtOH, 95–125 °C. (g) $POCl_3$, sulfolane, 107 °C. (h) NaOMe, $NH_4Cl$, MeOH, EtOH, 65 °C. (i) **1b**, DMF, $Et_3N$, 100 °C. (j) $H_2$ (60 bar), 5% Pd/C, DMF, 60 °C. (k) methyl chloroformate, *i*-PrOH, MeOH, then $Et_3N$, 50 °C.

**SAR and DMPK Optimization.** The SAR of the series of novel N-substituted methyl carbamates **1**–**8** was explored using a cGMP formation assay with sGC-overexpressing Chinese

hamster ovary (CHO) cells.[34] In addition, the metabolic stability of the compounds was assessed in vitro by incubation with rat hepatocytes. Initially, different carbamate N-substituents were tested with the aim of achieving higher metabolic stability than **1** while maintaining high potency (Table 1). Increasing steric bulk as in the ethyl derivative **2** had no beneficial effect on either potency or metabolic stability. The introduction of polarity (e.g., a hydroxyethyl functionality, as in **3**) led to a significant loss of potency relative to **1**, along with decreased metabolic stability. The next strategy, the introduction of fluorine atoms at the terminal position of the N-substituent, was designed to block metabolism. Interestingly, both the 2,2-difluoroethyl and 2,2,2-trifluoroethyl derivatives, **4** and **5**, exhibited high potency in the cGMP assay but had a 2–4.5-fold higher clearance in rat hepatocytes. *N*-Fluorobenzyl substitution revealed that the *ortho*-fluoro derivative **6** is significantly more potent (MEC = 0.1 μM) than the meta and para isomers, **7** and **8** (MEC = 0.2 and 0.7 μM, respectively). Nevertheless, all the benzylic derivatives had a high clearance in rat hepatocytes. These results and the testing of many further derivatives (data not shown) suggested that improving the metabolic stability by altering the N-substitution might be very difficult to achieve. Hence, optimization efforts were focused on the main metabolite of **1**, the *N*-desmethyl derivative **9**. This compound is less potent than **1** but displayed a somewhat higher metabolic stability in the rat hepatocyte assay, with a clearance of 0.1 L/h/kg. When tested in vivo in rats (iv dosing), compound **9** had a moderate clearance of 1.2 L/h/kg and a short half-life of only 1.2 hours.

**Table 1.** Properties of the N-Substituted Methyl Carbamates **1**–**8**

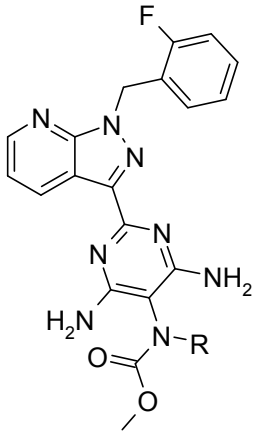

| Compd | R | cGMP formation MEC[a] [μM] | ClogD[35] pH 7.5 | In vitro clearance (rat hepatocytes) $CL_b$ [L/h/kg] |
|---|---|---|---|---|
| **1** |  | 0.03 | 1.99 | 0.2 |
| **2** |  | 0.2 | 2.29 | 0.7 |
| **3** | 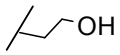 | 0.3 | 1.52 | 3.7 |
| **4** | 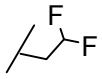 | 0.1 | 2.21 | 0.4 |
| **5** | 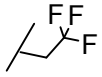 | 0.1 | 2.48 | 0.9 |
| **6** | 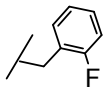 | 0.1 | 3.15 | 3.2 |
| **7** | 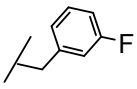 | 0.2 | 3.20 | 3.2 |
| **8** | 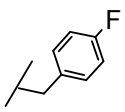 | 0.7 | 3.29 | 2.4 |

[a]MEC: Minimal effective concentration to achieve stimulation of cGMP formation (≥3-fold increase in basal luminescence) in a recombinant sGC-overexpressing cell line.[34]

Therefore, variations in the carbamate alkoxy group while leaving the N-position unsubstituted were examined next, with the goal of improving the half-life and other properties relative to compound **9** (Table 2).

The introduction of steric bulk in the form of an isopropyl residue (compound **10**) led to a strong decrease in potency relative to **9**, as well as decreased metabolic stability. Interestingly, there was increased potency with cyclobutyl derivative **11**; however, **11** was also unfavorable with respect to rat hepatocyte clearance. The oxetanyl group is well known in medicinal chemistry for improving metabolic stability[36, 37] over related alkyl derivatives. Remarkably, the exchange of cyclobutyl for oxetanyl (compound **12**) led to a 14-fold higher stability in rat hepatocytes, but sGC stimulation was weaker than with derivative **9** or **11**. Since the permeability across Caco-2 cell monolayers was also very low ($P_{app}$ A–B = 2 nm/s), combined with a high efflux ratio of 74, compound **12** was not pursued further. Additional efforts to improve the overall profile, by the introduction of fluorine or steric bulk (compounds **13** and **14**), led to a slight increase in potency (MEC = 0.2 μM vs 0.3 μM for **9**); however, metabolic stability was dramatically reduced.

**Table 2.** Properties of the N-H Alkyl Carbamates **9**–**14**

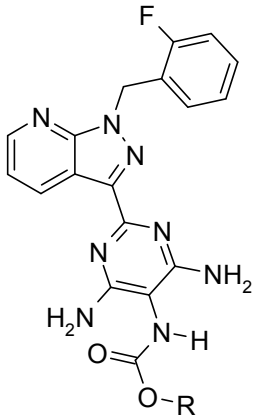


| Compd | R | cGMP | ClogD[35] | In vitro clearance (rat | Caco-2 |
|---|---|---|---|---|---|

| | | formation MEC[a] [μM] | pH 7.5 | hepatocytes) $CL_b$ [L/h/kg] | $P_{app}$ A–B [nm/s] (Efflux ratio) |
|---|---|---|---|---|---|
| **9** |  | 0.3 | 1.49 | 0.1 | 79 (5) |
| **10** |  | 0.8 | 2.10 | 0.9 | n.d.[b] |
| **11** |  | 0.2 | 2.05 | 1.4 | 23 (25) |
| **12** |  | 2.3 | 1.21 | 0.1 | 2 (74) |
| **13** |  | 0.2 | 2.05 | 2.1 | n.d.[b] |
| **14** |  | 0.2 | 2.09 | 1.4 | n.d.[b] |

[a]MEC: Minimal effective concentration to achieve stimulation of cGMP formation (≥3-fold increase in basal luminescence) in a recombinant sGC-overexpressing cell line.[34] [b]n.d.: not determined.

The oxazolidinone derivatives **15**–**18**, as conformationally fixed versions of the foregoing carbamates, were also studied to assess the influence of the constrained nature on sGC stimulation (Table 3). The parent oxazolidinone **15** was as equipotent as carbamate **9** and exhibited slightly decreased stability in rat hepatocytes. Intravenous dosing of compound **15** to rats resulted in a moderate clearance of 1.9 L/h/kg and a short half-life of about 1.0 hour, and thus **15** was not profiled further. Other attempts to increase metabolic stability by the introduction of steric bulk were unsuccessful, probably due to the more lipophilic[38] character of the resulting compounds **16**–**18**.

**Table 3.** Properties of the Oxazolidinones **15**–**18**

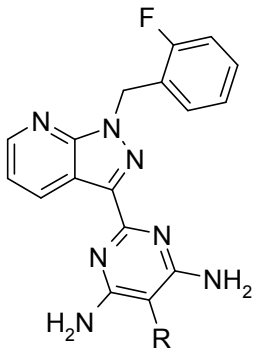

| Compd | R | cGMP formation MEC[a] [μM] | ClogD[35] pH 7.5 | In vitro clearance (rat hepatocytes) $CL_b$ [L/h/kg] |
|---|---|---|---|---|
| **15** | 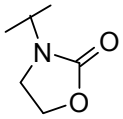 | 0.3 | 1.60 | 0.4 |
| **16** | 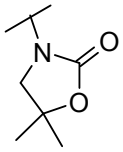 | 0.2 | 2.29 | 1.3 |
| **17** | 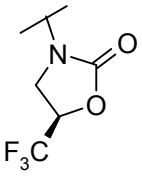 | 0.2 | 2.25 | n.d.[b] |
| **18** | 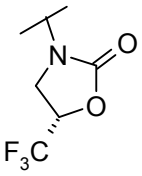 | 0.03 | 2.25 | 1.6 |

[a]MEC: Minimal effective concentration to achieve stimulation of cGMP formation (≥3-fold increase in basal luminescence) in a recombinant sGC-overexpressing cell line.[34] [b]n.d.: not determined.

In summary, although further optimization of the carbamate motif of **1** could not be achieved, a number of interesting and novel SAR observations were made, with the N-unsubstituted

carbamate **9** being identified as the most promising path forward. Thus, the focus of the optimization strategy was shifted away from the carbamate moiety and our efforts were directed to the central scaffold and the identification of alternative cores that could lead to superior overall pharmacokinetic profiles of the corresponding compounds.

Our studies with respect to central scaffold modifications are summarized in Table 4. Efforts were concentrated on novel core systems which had not been tested before in combination with 4,6-diaminopyrimidin-5-ylcarbamates.

Firstly, changes were made to the pyrazolo portion of the molecule, leading to the 1*H*-pyrazolo[4,3-*b*]pyridine derivative **19**. In addition to the benefit of a shorter synthetic route than that for compound **9**, **19** proved to be a moderately potent sGC stimulator with an MEC of 1.2 μM and had high metabolic stability when tested in rat hepatocytes. The introduction of substituents at the 6-position of the 1*H*-pyrazolo[4,3-*b*]pyridine core was, in general, not well tolerated leading to a dramatic loss of potency, with the exception of the 6-fluoro derivative **20** which exhibited an MEC of 0.5 μM and good metabolic stability. To our surprise, compounds **19** and **20** had very different in vivo clearances when compared in a rat pharmacokinetic experiment (iv dosing): fluoro derivative **20** had a low clearance of 0.3 L/h/kg versus 1.0 L/h/kg for compound **19**. As metabolite identification did not point to metabolism occurring at the pyridine core, the rationale for this threefold reduction in blood clearance remains unclear.

**Table 4.** Properties of the Core Variation Compounds **19**–**24**

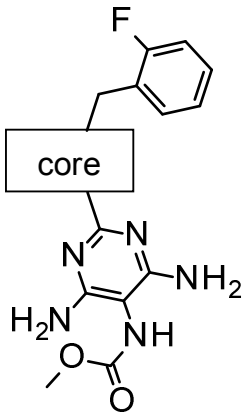


| Compd | Core | cGMP formation MEC[a] [μM] | In vitro clearance (rat hepatocytes) $CL_b$ [L/h/kg] | In vivo clearance (rat) $CL_b$ [L/h/kg] |
|---|---|---|---|---|
| **19** | 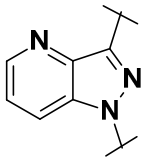 | 1.2 | <0.1 | 1.0 |
| **20** | 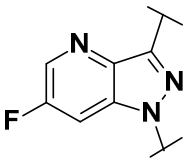 | 0.5 | 0.1 | 0.3 |
| **21** | 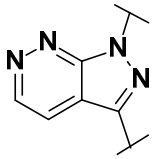 | 2.0 | <0.1 | 3.8 |
| **22** | 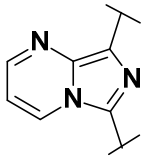 | 1.7 | n.d.[b] | 1.8 |
| **23** | 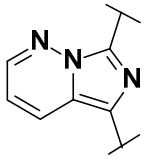 | 0.7 | <0.1 | 0.9 |

| | | | | |
|---|---|---|---|---|
| **24** | 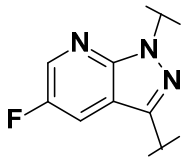 | 0.3 | 0.1 | 0.3 |

[a]MEC: Minimal effective concentration to achieve stimulation of cGMP formation (≥3-fold increase in basal luminescence) in a recombinant sGC-overexpressing cell line.[34] [b]n.d.: not determined.

Novel 1*H*-pyrazolo[3,4-*c*]pyridazine **21** proved to be a reasonably potent sGC stimulator but exhibited a high clearance of 3.8 L/h/kg when tested in vivo in rats and thus was not further profiled, along with imidazo[1,5-*a*]pyrimidine **22** for similar reasons. In contrast, imidazo[1,5-*b*]pyridazine **23** exhibited potent sGC stimulator properties (MEC = 0.7 μM), good metabolic stability in rat hepatocytes and a low to moderate clearance of 0.9 L/h/kg after intravenous dosing to rats. Finally, revisiting 1*H*-pyrazolo[3,4-*b*]pyridine **9** with an additional fluorine at the 5-position resulted in the potent sGC stimulator **24** (MEC = 0.3 μM) with good metabolic stability in rat hepatocytes and a surprisingly low clearance of 0.3 L/h/kg after intravenous dosing to rats (Table 4). Thus, the blood clearance of derivative **9** in rats (1.2 L/h/kg) was reduced fourfold by fluorination at position 5.

Finally, compounds **20**, **23** and **24** were selected for further pharmacokinetic profiling across species (Table 5). Fluoropyrazolo[3,4-*b*]pyridine derivative **24** exhibited the best overall pharmacokinetic profile by far, with a low clearance and long half-life in rats and dogs after intravenous dosing, as well as high oral bioavailability. In addition, **24** had no inhibitory effects on major CYP isoforms (1A2, 2A6, 2B6, 2C8, 2C9, 2C19, 2D6 and 3A4), as indicated by $IC_{50}$ values of >50 μM. Metabolite profiling in human hepatocytes was characterized by a low turnover, with glucuronide **25** (major) and debenzylated compound **26** (minor) being the only metabolites identified (Figure 1). Thus, the main biotransformation pathway shifted from

predominantly phase I oxidative CYP-mediated metabolism (**1**) to primarily phase II UGT-mediated conjugation with glucuronic acid.

**Table 5.** In vivo Pharmacokinetic Properties of **20**, **23**, **24** in comparison with **1**

| Compd | Species | $V_{ss}$ [L/kg] | $CL_b$ [L/h/kg] | $t_{1/2}$ [h] | Bioavailability [%] |
|---|---|---|---|---|---|
| **20** | rat | 0.5 | 0.3 | 1.5 | 26 |
| | dog | 1.0 | 0.2 | 4.1 | 56 |
| **23** | rat | 0.3 | 0.9 | 0.5 | 37 |
| | dog | 2.0 | 0.9 ($Cl_p$)[a] | 1.8 | n.d.[b] |
| **24** | rat | 1.0 | 0.3 | 3.4 | 65 |
| | dog | 1.4 | 0.2 | 6.2 | 75 |
| **1** | rat | 1.2 | 1.3 | 1.4 | 46 |
| | dog | 0.7 | 0.3 ($Cl_p$)[a] | 2.4 | 79 |

[a]$Cl_p$: Plasma clearance. [b]n.d.: not determined.

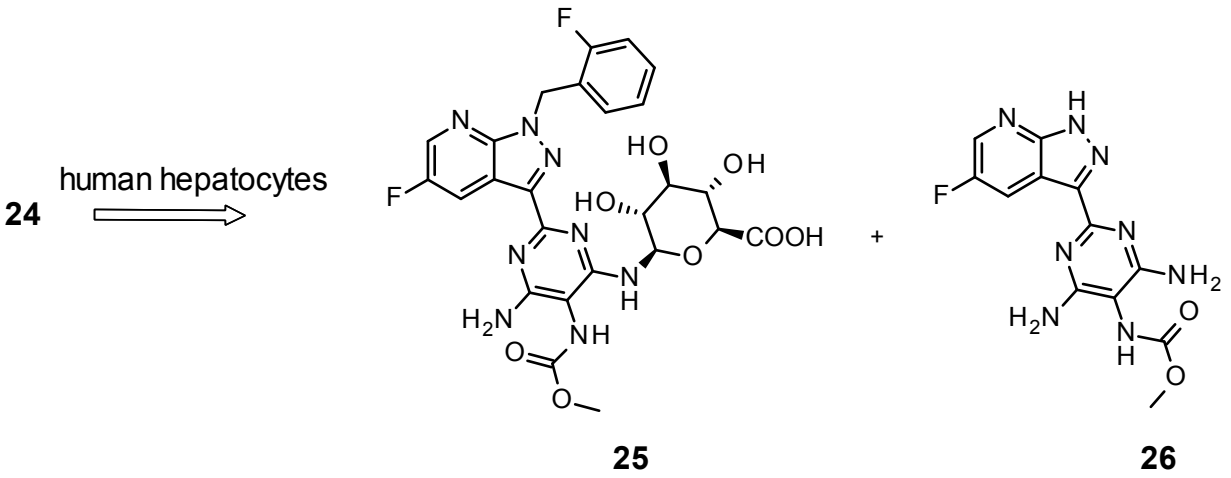


**Figure 1.** Biotransformation products of **24** in human hepatocytes.

**Pharmacology. 24** was extensively profiled preclinically in vitro, on the isolated sGC enzyme and on isolated vessels, ex vivo in isolated hearts and in vivo in a rat model of cardiovascular disease associated with cardiorenal syndrome.

**Highly Purified Recombinant sGC.** Studies on the in vitro effects of **24** on highly purified sGC revealed that **24** (0.01 μM to 100 μM) stimulates recombinant sGC concentration-dependently, by 1.7-fold to 57.6-fold (Figure 2). When combined with the NO donor diethylamine/nitric oxide complex (DEA/NO), **24** and DEA/NO had a synergistic effect on the enzyme activity over a wide range of concentrations. At highest concentrations of **24** (100 μM) and DEA/NO (100 nM), the specific activity of sGC was 341.6-fold above baseline (Figure 2). Moreover, the effects of **24** in the presence of the sGC inhibitor 1*H*-[1,2,4]oxadiazolo[4,3-*a*]quinoxalin-1-one (ODQ) were evaluated. The sGC stimulation induced by **24** was nearly completely blocked by ODQ, and reduced to 18-fold (Figure 2). Thus, **24** exhibits all the characteristics of a potent and selective sGC stimulator, stimulating sGC NO-independently and in synergy with NO. In addition, **24** predominantly acts on the heme-containing nonoxidized form of sGC.

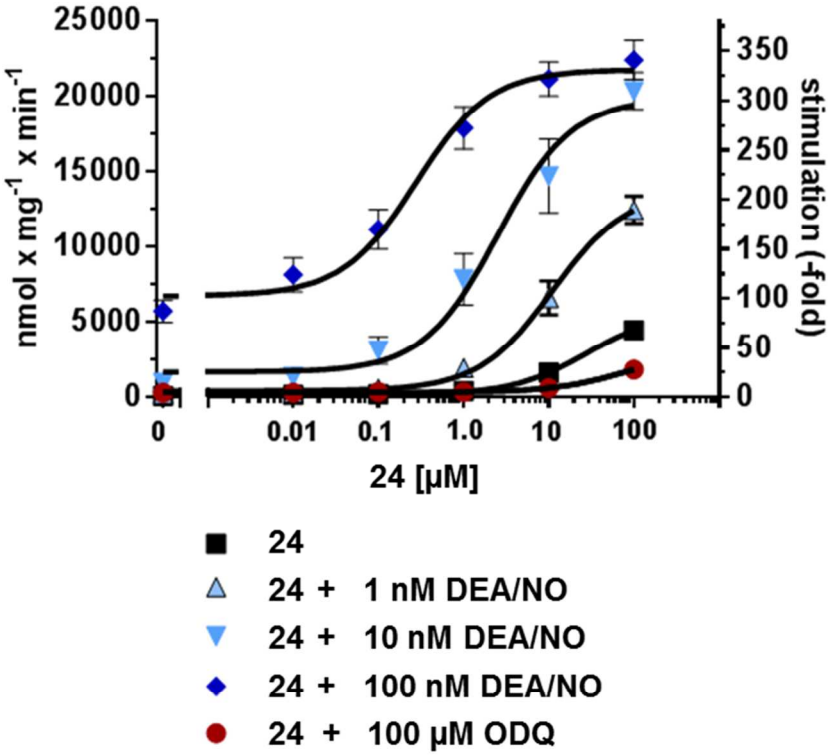


**Figure 2.** Effects of **24** and NO on the stimulation of highly purified sGC, and blocking effects of the sGC inhibitor ODQ.

**sGC-Overexpressing Cells.** The stimulation of sGC by **24** was examined with a recombinant CHO cell line overexpressing rat sGC. **24** stimulated the sGC reporter cell line concentration-dependently, with an $EC_{50}$ of 1005 ± 145 nM. In the presence of the NO donor *S*-nitroso-*N*-acetyl-D,L-penicillamine (SNAP) (30 and 100 nM), the $EC_{50}$ value shifted to 39.0 ± 5.1 nM and 10.6 ± 1.7 nM, respectively. In the presence of ODQ, pretreatment of the sGC reporter cell line with 10 µM ODQ for 3 hours resulted in a significantly reduced efficacy of **24**, with an $EC_{50}$ of 256 ± 40 nM being observed.

**Isolated Vessels and Tolerance. 24** inhibited phenylephrine-induced contractions of rabbit saphenous artery rings, rabbit aortic rings and canine femoral vein rings concentration-

dependently, with $IC_{50}$ values of 798 nM, 692 nM and 3072 nM, respectively. In addition, **24** inhibited the U46619-induced contractions of porcine coronary artery rings concentration-dependently, with an $IC_{50}$ of 956 nM.

Chronic administration of organic nitrates leads to the rapid development of nitrate tolerance. Thus, the vasorelaxant effect of **24** on isolated saphenous artery rings taken from normal and nitrate-tolerant rabbits was examined. Treatment with isosorbide dinitrate for 3–4 days resulted in a marked inhibition of glycerol trinitrate (GTN) mediated vasodilation. GTN inhibited phenylephrine-induced contractions with an $IC_{50}$ of 1.9 nM in control vessels and an $IC_{50}$ of 9.6 nM in tolerant vessels, confirming the presence of nitrate tolerance. In contrast to GTN, **24** is a potent inhibitor of phenylephrine-induced contractions both in normal and nitrate-tolerant saphenous artery rings, with $IC_{50}$ values of 5.6 nM and 5.8 nM, respectively.

**Langendorff-Perfused Hearts.** In rat heart Langendorff preparations, ex vivo, **24** reduced the coronary perfusion pressure in a concentration-dependent manner (Figure 3). Up to the highest concentration tested, **24** had no effect on heart rate, left ventricular diastolic pressure and contractility.

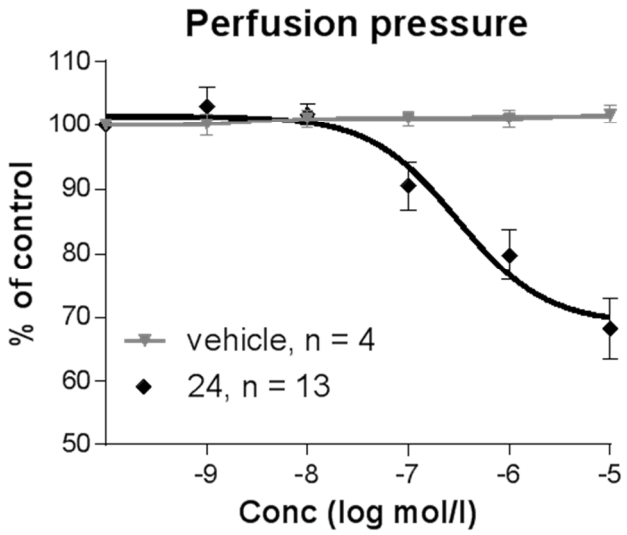


**Figure 3.** Effects of **24** on rat heart Langendorff preparations.

**Long-Term Study with L-NAME-Treated Renin Transgenic Rats.** The potential impact on cardiovascular health of the stimulation of sGC was evaluated by determining the long-term effects of **24** on hemodynamic and hormonal parameters in renin transgenic rats (RenTG) carrying the additional mouse renin gene (mRenR2)27. These RenTG(mRenR2)27 rats were additionally treated with the NO synthase inhibitor $N_{\omega}$-nitro-L-arginine methyl ester (L-NAME) in the drinking water. This well-established rodent disease model is characterized by hypertension, heart and kidney failure, and increased mortality.[39] The RenTG(mRenR2)27/L-NAME-supplemented rats were chronically treated with either placebo (2 mL/kg q.d.), which served as the control group, or **24** (3 or 10 mg/kg q.d.).

**Effects on Blood Pressure and on the Heart.** Chronic oral treatment with 3 or 10 mg/kg **24** q.d. resulted in a significant attenuation of blood pressure increase during the course of the study. However, the overall rise of blood pressure increase was not halted in the 3 and 10 mg/kg treatment groups (Figure 4).

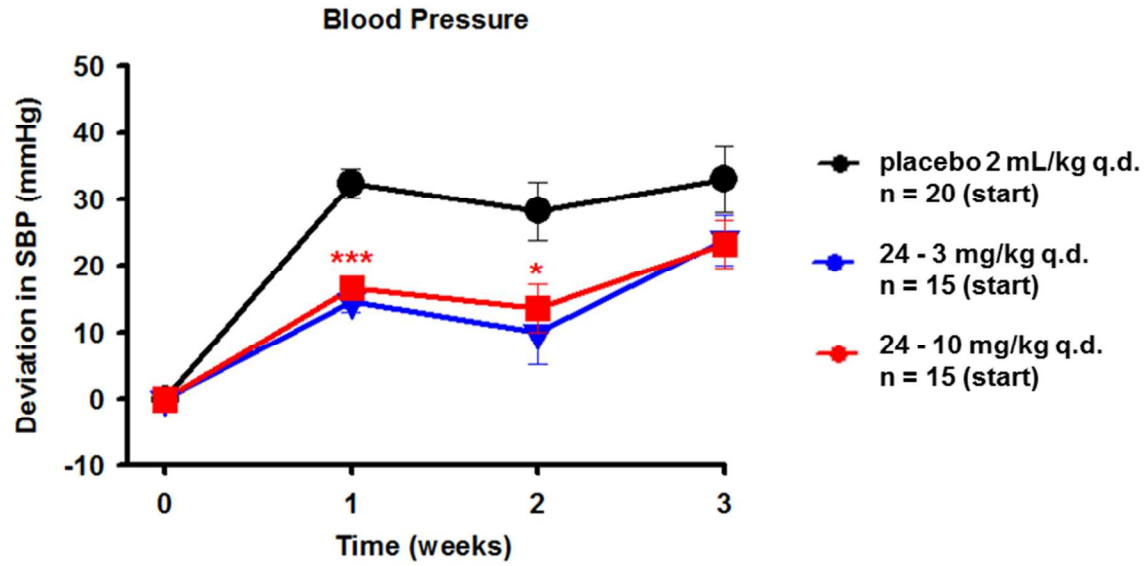


**Figure 4.** Increase in systolic blood pressure in mmHg during the course of the study with L-NAME-treated renin transgenic rats.

In addition, a significant and dose-dependent reduction of heart hypertrophy, in both the right and left ventricle, was found in the 3 and 10 mg/kg treatment groups compared to the placebo group (Figure 5). Furthermore, plasma ANP levels decreased significantly in both treatment groups, also suggesting a functional improvement of the heart.

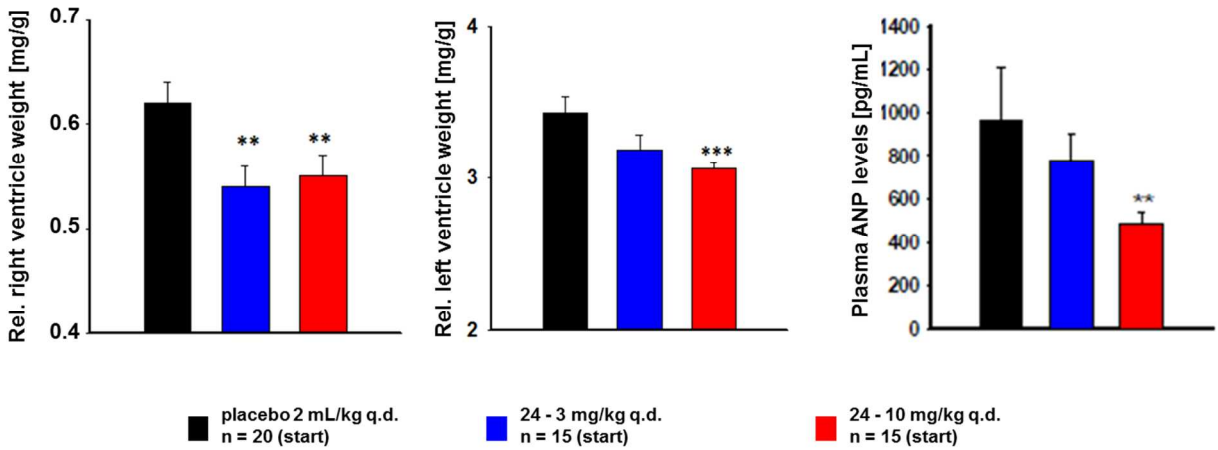

**Figure 5.** Right and left ventricle weight normalized on body weight (left/middle) and plasma atrial natriuretic peptide levels [in pg/mL] at the study end, after 3 weeks of treatment.

**Effects on the Kidneys.** With respect to kidney damage, **24** treatment at 3 or 10 mg/kg led to a significant reduction in kidney injury molecule Kim-1 and osteopontin expression which are used as biomarkers for renal injury and dysfunction (data not shown). In addition, proteinuria was significantly and dose-dependently decreased in the treatment groups, also suggesting a functional improvement of the kidneys (Figure 6).

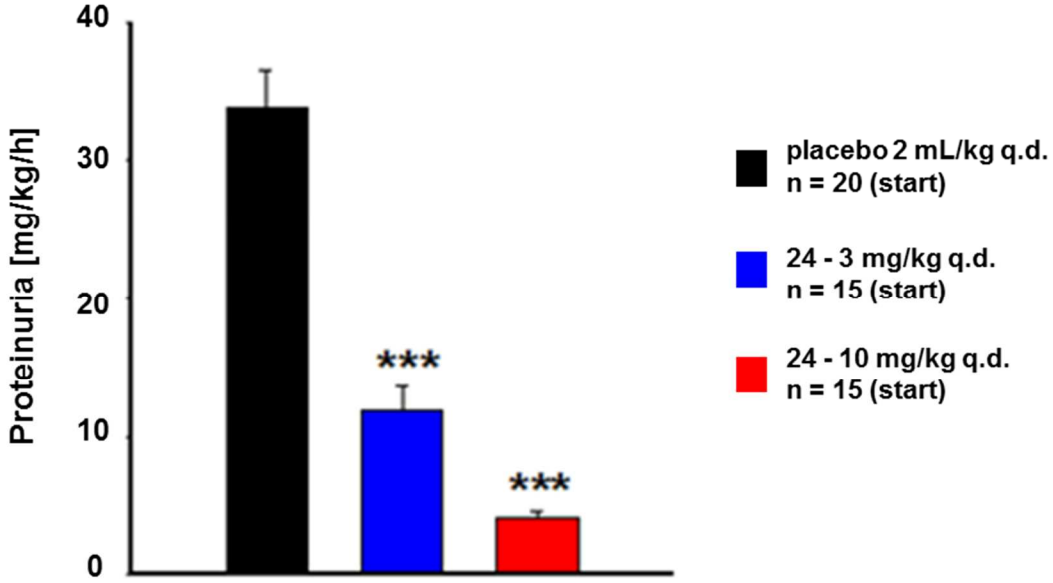


**Figure 6.** Effects on proteinuria at the study end, after 3 weeks of treatment.

**Effects on Mortality.** Treatment with **24** resulted in a significant and dose-dependent increase in survival rates. In the 3 and 10 mg/kg q.d. treatment groups, the rat survival rate was 70% and 90%, respectively, at the study end. In contrast, the survival rate in the placebo group was only 25% after 21 days (Figure 7).

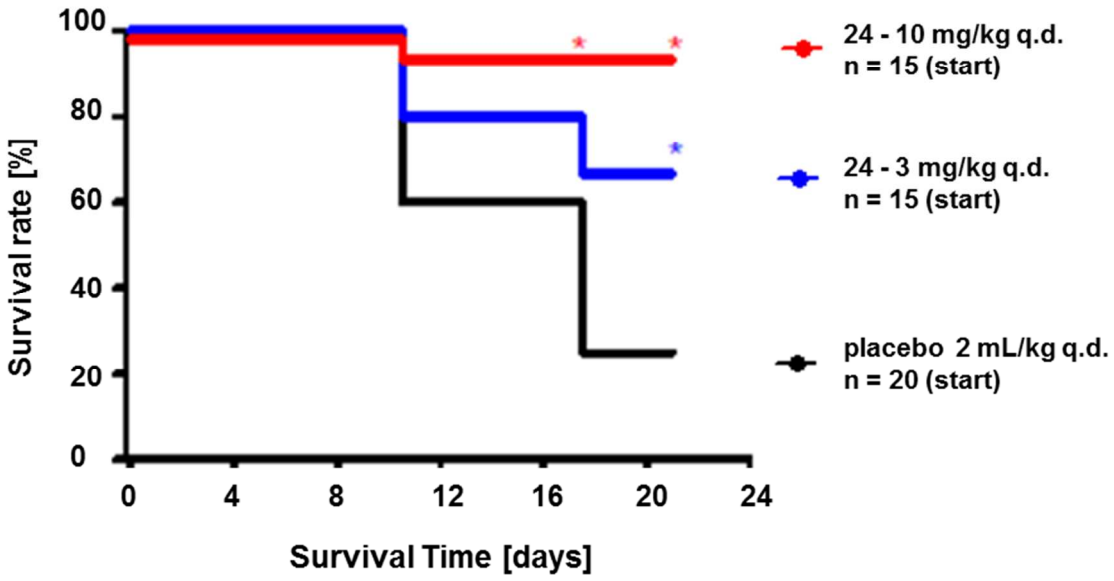


**Figure 7.** Kaplan–Meier survival curves.

These in vivo data strongly suggest that the sGC stimulator **24** can maintain heart and kidney function in a model of hypertension-induced end-organ damage, with substantially reduced overall mortality, strongly suggesting a beneficial role of **24** for the treatment of cardiovascular diseases associated with cardiorenal syndrome.[40]

## CONCLUSION

In summary, we have identified **24** as a potent, orally available stimulator of sGC. Our optimization work starting from **1** led to the identification of compounds with superior in vitro and in vivo pharmacokinetic and metabolic profiles. **24**, the compound with the best overall profile from these preclinical studies, was selected as clinical candidate and proved to have a pharmacokinetic profile in humans suitable for once daily dosing. Additional in vivo studies in animal models of hypertension, heart failure and kidney disease have revealed dose-dependent

antifibrotic and organ-protective properties in line with the sGC stimulator mode of action. **24** is currently being investigated in a phase 3 clinical trial in HFrEF patients.

## EXPERIMENTAL SECTION

### Chemistry

**General Procedures.** Unless otherwise noted, all nonaqueous reactions were carried out under an argon atmosphere with commercial-grade reagents and solvents. All final products were at least 95% pure, as determined by analytical HPLC.

$^1$H NMR spectra were recorded on Bruker Avance spectrometers operating at 400 or 500 MHz. Chemical shifts (δ) are reported in ppm relative to TMS as an internal standard and coupling constants (*J*) are given in hertz (Hz). Spin multiplicities are reported as s = singlet, br s = broad singlet, d = doublet, dd = doublet of doublets, t = triplet, q = quartet, m = multiplet. LC-MS analysis was performed using the respective method a–d, as noted. Method a: instrument: Micromass TOF-MUX interface 4× parallel injection with Waters 600 HPLC; column: Phenomenex Synergi 2 μm Hydro-RP Mercury 20 × 4 mm; mobile phase A: $H_2O$ (1 L) + 50% formic acid (0.5 mL), mobile phase B: MeCN (1 L) + 50% formic acid (0.5 mL); gradient: 0.0 min 90% A → 2.5 min 30% A → 3.0 min 5%A → 4.5 min 5% A; oven: 20 °C; flow: 1 mL/min; UV detection: 210 nm. Method b: instrument: Micromass Quattro Premier with Waters Acquity UPLC; column: Thermo Hypersil GOLD 1.9 μm, 50 × 1 mm; mobile phase A: $H_2O$ (1 L) + 50% formic acid (0.5 mL), mobile phase B: MeCN (1 L) + 50% formic acid (0.5 mL); gradient: 0.0 min 90% A → 0.1 min 90% A → 1.5 min 10% A → 2.2 min 10% A; oven: 50 °C; flow: 0.33 mL/min; UV detection: 210 nm. Method c: instrument: Waters Micromass Quattro Micro with Agilent 1100 series HPLC; column: Thermo Hypersil GOLD 3 μm, 20 × 4 mm; mobile phase A:

$H_2O$ (1 L) + 50% formic acid (0.5 mL), mobile phase B: MeCN (1 L) + 50% formic acid (0.5 mL); gradient: 0.0 min 100% A → 3.0 min 10% A → 4.0 min 10% A; oven: 50 °C; flow: 2 mL/min; UV detection: 210 nm. Method d: instrument: Waters Acquity SQD UPLC system; column: Waters Acquity UPLC HSS T3 1.8 μm, 50 × 1 mm; mobile phase A: $H_2O$ (1 L) + 99% formic acid (0.25 mL), mobile phase B: MeCN (1 L) + 99% formic acid (0.25 mL); gradient: 0.0 min 90% A → 1.2 min 5% A → 2.0 min 5% A; oven: 50 °C; flow: 0.4 mL/min; UV detection: 208–400 nm.

**Materials.** Intermediates **1a–c,**[25] **3b**,[33] **4h**[41] and compounds **1**,[25] **2**,[42] **4–8**,[43] **9**,[44] **10**,[44] **11–14**,[45] **15–18**,[43] **19**,[46] **20**[47] and **23**[48] were synthesized according to the methods described previously.

**Methyl {4,6-Diamino-2-[1-(2-fluorobenzyl)-1*H*-pyrazolo[3,4-*b*]pyridin-3-yl]pyrimidin-5-yl}(2-hydroxyethyl)carbamate (3). 1c** (200 mg, 0.57 mmol) and AcOH (33 μL, 0.57 mmol) were dissolved in MeOH (20 mL) and the mixture was cooled to 0 °C. Then, a solution of glycolaldehyde (34 mg, 0.57 mmol) in MeOH (20 mL) was added dropwise. After complete addition, the mixture was stirred for a further 15 min at 0 °C. Then, $NaBH_3CN$ (50 mg, 0.80 mmol) was added portionwise. The mixture was stirred at rt for 20 h and then concentrated under reduced pressure. The residue was diluted with EtOAc and washed with concd aq $NH_4Cl$ solution. The organic layer was concentrated under reduced pressure and the residue was purified by HPLC (MeCN/$H_2O$ gradient) to give 2-({4,6-diamino-2-[1-(2-fluorobenzyl)-1*H*-pyrazolo[3,4-*b*]pyridin-3-yl]pyrimidin-5-yl}amino)ethanol (**1d**) as a yellow solid. Yield: 165 mg (73%). $^1$H NMR (400 MHz, [$D_6$]DMSO): δ = 9.04 (dd, *J* = 8.1, 1.7 Hz, 1H), 8.58 (dd, *J* = 4.7, 1.7 Hz, 1H), 7.27–7.39 (m, 2H), 7.22 (dd, *J* = 10.0, 8.8 Hz, 1H), 7.08–7.16 (m, 2H), 6.09 (br s, 4H), 5.77 (s, 2H), 4.77 (t, *J* = 5.1 Hz, 1H), 3.47 (td, *J* = 5.6, 5.1 Hz, 2H), 3.27 (t, *J* = 6.4 Hz, 1H),

2.83 (dt, $J$ = 6.4, 5.6 Hz, 2H). LC-MS (method a): $^{t}$R (min) = 1.27. MS (EI+): $m/z$ = 395 $[M + H]^+$.

**1d** (265 mg, 0.67 mmol) was dissolved in pyridine (5.0 mL) and the solution was cooled to 0 °C. Methyl chloroformate (83 mg, 0.87 mmol) was added and the mixture was stirred at rt overnight. Then, the mixture was concentrated under reduced pressure and the residue was purified by preparative HPLC ($H_2O$/MeCN/1% TFA 56:30:14) to give **3** as a white solid. Yield: 37 mg (12%). $^1$H NMR (500 MHz, [$D_6$]DMSO): δ = 9.04 (dd, $J$ = 8.0, 1.5 Hz, 1H), 8.59 (dd, $J$ = 4.5, 1.5 Hz, 1H), 7.34–7.38 (m, 1H), 7.32 (dd, $J$ = 8.0, 4.5 Hz, 1H), 7.22 (dd, $J$ = 10.0, 8.8 Hz, 1H), 7.09–7.15 (m, 2H), 6.07 (br s, 4H), 5.78 (s, 2H), 4.14 (t, $J$ = 5.7 Hz, 2H), 3.70 (s, 3H), 3.54 (t, $J$ = 7.0 Hz, 1H), 3.00 (dt, $J$ = 7.0, 5.7 Hz, 2H). LC-MS (method a): $^{t}$R (min) = 1.49. MS (EI+): $m/z$ = 453 $[M + H]^+$.

**3-Bromo-1*H*-pyrazolo[3,4-*c*]pyridazine (3c).** 1*H*-Pyrazolo[3,4-*c*]pyridazin-3-ol[33] (**3b**; 18.00 g, 132.24 mmol) was dissolved in sulfolane (176 mL), and $POBr_3$ (39.81 g, 138.85 mmol) was then added to the solution. The mixture was stirred at 150 °C for 3 h. After being cooled to rt, the mixture was poured onto ice–water and extracted with EtOAc (3 ×). The combined organic extracts were washed with $H_2O$ and brine, dried over $Na_2SO_4$, filtered and concentrated until a precipitate formed. The solids were collected by filtration and dried under reduced pressure. Yield: 16.27 g (62%). $^1$H NMR (400 MHz, [$D_6$]DMSO): δ = 14.90 (br s, 1H), 9.23 (d, $J$ = 5.6 Hz, 1H), 8.10 (d, $J$ = 5.6 Hz, 1H). LC-MS (method b): $^{t}$R (min) = 1.15. MS (ESI+): $m/z$ = 199 $[M + H]^+$.

**3-Bromo-1-(2-fluorobenzyl)-1*H*-pyrazolo[3,4-*c*]pyridazine (3d). 3c** (16.27 g, 81.75 mmol) and $Cs_2CO_3$ (31.97 g, 98.10 mmol) were mixed in DMF (150 mL). A solution of 2-fluorobenzyl

bromide (17.00 g, 89.93 mmol) in DMF (50 mL) was then added dropwise and the mixture was stirred at rt overnight. The mixture was then diluted with EtOAc (500 mL) and washed with $H_2O$ (3 ×) and brine (1 ×). The organic phase was separated, dried over $MgSO_4$, filtered and concentrated. The residue was purified by flash column chromatography on silica gel (DCM/MeOH gradient). The obtained crude product was triturated with MTBE and DCM, collected by filtration, washed with MTBE and dried under reduced pressure. Yield: 11.36 g (45%). $^1$H NMR (400 MHz, [D$_6$]DMSO): δ = 9.30 (d, *J* = 5.6 Hz, 1H), 8.15 (d, *J* = 5.6 Hz, 1H), 7.35–7.44 (m, 2H), 7.16–7.28 (m, 2H), 5.96 (s, 2H). LC-MS (method c): $^t$R (min) = 1.11. MS (ESI+): *m*/*z* = 307 $[M + H]^+$.

**1-(2-Fluorobenzyl)-1*H*-pyrazolo[3,4-*c*]pyridazine-3-carbonitrile (3e). 3d** (1.00 g, 3.26 mmol) and CuCN (0.32 g, 3.58 mmol) were treated with anhyd DMSO (10 mL) and the mixture was stirred at 150 °C for 9 h. The mixture was brought to rt, then poured onto ice–water and treated with 25% aq $NH_4OH$ until all solids were dissolved (blue solution). The mixture was then extracted with EtOAc (3 ×). The combined organic extracts were dried over $Na_2SO_4$, filtered and concentrated. The residue was purified by flash column chromatography on silica gel (cyclohexane/EtOAc 4:1) to give the crude product which was used without further purification. Yield: 0.57 g (51%, purity 74%). $^1$H NMR (400 MHz, [D$_6$]DMSO): δ = 9.45 (d, *J* = 5.9 Hz, 1H), 8.50 (d, *J* = 5.9 Hz, 1H), 7.39–7.51 (m, 2H), 7.18–7.30 (m, 2H), 6.11 (s, 2H). LC-MS (method d): $^t$R (min) = 0.94. MS (ESI+): *m*/*z* = 254 $[M + H]^+$.

**1-(2-Fluorobenzyl)-1*H*-pyrazolo[3,4-*c*]pyridazine-3-carboximidamide (3f). 3e** (1.19 g, 4.70 mmol) and NaOMe (0.96 g, 17.86 mmol) were treated with anhyd MeOH (31 mL), and the mixture was stirred at rt for 2 h. $NH_4Cl$ (0.30 g, 5.64 mmol) and AcOH (1.05 mL) were then

added and the mixture was stirred under reflux overnight. The mixture was then concentrated and the residue was taken up in EtOAc and 1 M aq NaOH. The organic phase was separated, washed with 1 M aq NaOH, dried over $Na_2SO_4$, filtered and concentrated. The solid residue was triturated with MTBE, collected by filtration, washed with DCM/MeOH (50:1) and dried under reduced pressure. Yellow solid; yield: 0.43 g (34%). $^1$H NMR (400 MHz, [$D_6$]DMSO): δ = 9.26 (d, *J* = 5.1 Hz, 1H), 8.48 (d, *J* = 5.1 Hz, 1H), 7.38 (d, *J* = 5.9 Hz, 1H), 7.11–7.32 (m, 3H), 6.71 (br s, 2H), 5.99 (s, 2H). LC-MS (method c): $^t$R (min) = 0.52. MS (ESI+): *m*/*z* = 271 $[M + H]^+$.

**2-[1-(2-fluorobenzyl)-1*H*-pyrazolo[3,4-*c*]pyridazin-3-yl]-5-[(*E*)-phenyldiazenyl]pyrimidine-4,6-diamine (3i).** Aniline (0.202 mL, 2.22 mmol) was dissolved in $H_2O$ (2.0 mL) and the solution was cooled to 0 °C. Aq HCl (37%, 0.38 mL) was then added dropwise followed by a solution of $NaNO_2$ (153 mg, 2.22 mmol) in $H_2O$ (0.5 mL). The mixture was stirred for an additional 15 min and a solution of NaOAc (231 mg, 2.82 mmol) in $H_2O$ (0.5 mL) was then added dropwise followed by a solution of malononitrile (147 mg, 2.22 mmol) in EtOH (3.0 mL). The mixture was then stirred for an additional 2 h at 0 °C. The resulting precipitate was collected by filtration, washed with $H_2O$ (3 ×) and then dissolved in DMF (5.0 mL). In a separate flask, **3f** (599 mg, 2.22 mmol) was dissolved in DMF (5.0 mL), then $Et_3N$ (0.309 mL, 2.22 mmol) was added dropwise. The mixture was warmed to 85 °C and the aforementioned DMF solution was added. The resulting mixture was stirred at 100 °C overnight, then cooled to 0 °C and treated with $H_2O$. The formed solids were collected by filtration, washed with $H_2O$ and MeOH, and dried to give 2-[1-(2-fluorobenzyl)-1*H*-pyrazolo[3,4-*c*]pyridazin-3-yl]-5-[(*E*)-phenyldiazenyl]pyrimidine-4,6-diamine as a yellow solid. Yield: 0.68 g (68%). $^1$H NMR (400 MHz, [$D_6$]DMSO): δ = 9.35 (d, *J* = 5.4 Hz, 1H), 9.01 (d, *J* = 5.6 Hz, 1H), 8.54 (br s, 2H), 7.89–

8.07 (m, $J$ = 7.8 Hz, 4H), 7.45–7.54 (m, 2H), 7.31–7.44 (m, 3H), 7.16–7.30 (m, 2H), 6.06 (s, 2H). LC-MS (method d): $^{t}$R (min) = 1.08. MS (ESI+): $m/z$ = 441 $[M + H]^+$.

**2-[1-(2-fluorobenzyl)-1*H*-pyrazolo[3,4-*c*]pyridazin-3-yl]pyrimidine-4,5,6-triamine (3h). 3i** (300 mg, 0.68 mmol) was suspended in DMF (15 mL) and 10% Pd/C (58 mg) was added. The mixture was stirred in an $H_2$ atmosphere at ambient pressure overnight. The solids were collected by filtration and washed with MeOH and DCM, and the filtrate was concentrated under reduced pressure. The residue was triturated with DCM, and the solids were collected by filtration and dried under reduced pressure at 50 °C to give 2-[1-(2-fluorobenzyl)-1*H*-pyrazolo[3,4-*c*]pyridazin-3-yl]pyrimidine-4,5,6-triamine. The crude product was used without further purification. Yield: 198 mg (74%, purity 90%). LC-MS (method d): $^{t}$R (min) = 1.08. MS (ESI+): $m/z$ = 352 $[M + H]^+$.

**2-[8-(2-fluorobenzyl)imidazo[1,5-*a*]pyrimidin-6-yl]-5-[(*E*)-phenyldiazenyl]pyrimidine-4,6-diamine (4i).** 8-(2-Fluorobenzyl)imidazo[1,5-*a*]pyrimidine-6-carboximidamide[41] (**4h**; 70% purity, 1.30 g, 3.40 mmol) was mixed with DMF (24.6 mL) and $Et_3N$ (0.52 mL, 3.74 mmol). At 85 °C, a solution of [(*E*)-phenyldiazenyl]malononitrile (**1b**; 694 mg, 4.08 mmol) in DMF (12.0 mL) was added dropwise and the mixture was stirred for an additional 15 h at 100 °C. The resulting mixture was then poured into $H_2O$ (300 mL) and the resulting precipitate was collected by filtration, washed with $H_2O$ and dried. Then, MeCN (160 mL) was added and the remaining solids were collected by filtration and dried again to give 2-[8-(2-fluorobenzyl)imidazo[1,5-*a*]pyrimidin-6-yl]-5-[(*E*)-phenyldiazenyl]pyrimidine-4,6-diamine. Yield: 419 mg (28%). $^1$H NMR (400 MHz, [$D_6$]DMSO): δ = 10.23–10.31 (m, 1H), 9.42 (br s, 1H), 8.60–8.66 (m, 1H), 8.12 (d, $J$ = 7.6 Hz, 2H), 7.51–7.58 (m, 2H), 7.44–7.50 (m, 1H), 7.23–7.36 (m, 3H), 7.15–7.23

(m, 1H), 7.08–7.15 (m, 1H), 4.44 (s, 2H). LC-MS (method c): $^{t}$R (min) = 1.14. MS (ESI+): *m*/*z* = 440 $[M + H]^+$.

**2-[8-(2-fluorobenzyl)imidazo[1,5-*a*]pyrimidin-6-yl]pyrimidine-4,5,6-triamine (4j). 4i** (100 mg, 0.228 mmol) was dissolved in DMF (11.4 mL) and MeOH (2.9 mL). The solution was cooled with ice and then 10% Pd/C (20 mg) was added. The mixture was stirred at 0 °C under 1 atmosphere of $H_2$ for 48 h. The resulting mixture was filtered through Celite and the solids were washed with MeOH. The combined filtrate was concentrated under reduced pressure to give crude 2-[8-(2-fluorobenzyl)imidazo[1,5-*a*]pyrimidin-6-yl]pyrimidine-4,5,6-triamine which was purified by preparative reversed-phase HPLC ($H_2O$ + 0.1% $NH_3$/MeCN gradient). Brown solid; yield: 36 mg (45%). $^1$H NMR (400 MHz, [$D_6$]DMSO): δ = 10.13 (br d, *J* = 7.4 Hz, 1H), 8.20 (br d, *J* = 3.9 Hz, 1H), 7.19–7.31 (m, 2H), 7.04–7.17 (m, 2H), 6.81 (dd, *J* = 3.7, 7.6 Hz, 1H), 5.89 (s, 4H), 4.27 (s, 2H), 4.06 (s, 2H). LC-MS (method d): $^{t}$R (min) = 0.74. MS (ESI+): *m*/*z* = 351 $[M + H]^+$.

**4-(2,2,3,3-Tetrafluoropropyl)morpholine (6b).** $Tf_2O$ (252.5 g, 0.895 mol) was heated to 40 °C and, at this temperature, 2,2,3,3-tetrafluoro-1-propanol (**6a**; 130.0 g, 0.984 mol) was metered in while cooling. After the addition was completed, the mixture was heated to 70–75 °C and stirred for 2 h. Then, the mixture was cooled to 20 °C and the reaction solution of 2,2,3,3-tetrafluoropropyl trifluoromethanesulfonate was used without further purification.

Morpholine (158.5 g, 1.82 mol) was cooled to 5 °C. At 5–10 °C, the reaction solution of the triflate (189.5 g, max 0.455 mol) was added dropwise while cooling and then the mixture was stirred at 5–10 °C for 30 min. Then, the mixture was heated to 40 °C and stirred for 1 h. After cooling to 20 °C, $H_2O$ (160 mL) and toluene (160 mL) were added and the phases were

separated. The organic phase was washed with $H_2O$ (160 mL) and concentrated on a rotary evaporator at 50 °C/50 mbar. The residue (81.0 g) was distilled at 67–68 °C/18 mbar to give **6b**. Yield: 77.0 g (84%). $^1$H NMR (400 MHz, $CDCl_3$): δ = 5.83–6.22 (m, 1H), 3.61–3.78 (m, 4H), 2.89 (tt, *J* = 14.0, 1.7 Hz, 2H), 2.53–2.70 (m, 4H).

**4-Methyl-4-(2,2,3,3-tetrafluoropropyl)morpholin-4-ium Methanesulfonate (6c).** Methyl methanesulfonate (143.7 g, 1.31 mol) was heated to 135 °C and, at this temperature, **6b** (250.0 g, 1.24 mol) was added dropwise. The mixture was stirred at 100 °C for 22 h, then cooled to 85 °C and *i*-PrOH (375 mL) was added. After cooling to 0–5 °C, the mixture was stirred for a further 30 min. The product was collected by suction filtration, washed with *i*-PrOH (3 × 125 mL) and dried at 45 °C under a gentle $N_2$ stream in a vacuum drying cabinet. Yield: 336.8 g (87%). $^1$H NMR (400 MHz, $D_2O$): δ = 6.13–6.48 (m, 1H), 4.33–4.51 (m, 2H), 4.01–4.24 (m, 4H), 3.68–3.93 (m, 4H), 3.55 (s, 3H), 2.81 (s, 3H).

**4-Methyl-4-(2,3,3-trifluoroprop-1-enyl)morpholin-4-ium Methanesulfonate (6d).** 45% aq NaOH (16.9 g, 189.9 mmol) was metered into a solution of **6c** (53.8 g, 172.7 mol) in $H_2O$ (40 mL) at 50–55 °C, and the mixture was stirred at 50 °C for 1 h then cooled to 20 °C. The precipitated salts were removed by suction filtration and washed with $H_2O$ (5 mL). The aqueous solution of product **6d** (102.1 g, max 172.7 mmol) was used in the next stage. For analytical purposes, a sample was concentrated and dried. $^1$H NMR (400 MHz, $D_2O$): δ = 6.74–6.83 (m, 1H), 6.39–6.69 (m, 1H), 4.12–4.20 (m, 2H), 3.97–4.09 (m, 4H), 3.76–3.85 (m, 2H), 3.59 (s, 3H), 2.81 (s, 3H).

**2-Fluoro-3-(morpholin-4-yl)acrylaldehyde (6e).** A mixture of morpholine (30.2 g, 345.3 mmol) and $Et_3N$ (52.5 g, 518.0 mmol) was heated to 75 °C and the aqueous solution of **6d** (max

172.7 mmol) was added dropwise at 75–80 °C. The mixture was stirred under reflux for 2 h, cooled to 23 °C and washed with DCM (100 mL). The aqueous phase was washed twice with DCM/$Et_3N$ (100:15, 115 mL) and the combined organic phases were washed with sat. aq $K_2CO_3$ solution (85 mL) and concentrated under reduced pressure at 45–50 °C. Toluene (120 mL) was added, then toluene (60 mL) was distilled off. The suspension was stirred at rt overnight and the product was collected by suction filtration and dried at 50 °C under a gentle $N_2$ stream in a vacuum drying cabinet. Yield: 19.2 g (68%). $^1$H NMR (500 MHz, $CDCl_3$): δ = 8.59 (d, *J* = 18.9 Hz, 1H), 6.16 (d, *J* = 27.1 Hz, 1H), 3.72–3.83 (m, 4H), 3.51–3.60 (m, 4H).

**Ethyl 5-Fluoro-1-(2-fluorobenzyl)-1*H*-pyrazolo[3,4-*b*]pyridine-3-carboxylate (6f).** Ethyl 5-amino-1-(2-fluorobenzyl)-1*H*-pyrazole-3-carboxylate[49] (22.3 g, 84.8 mmol) was initially charged into EtOH (59.5 mL), and MsOH (11.0 mL, 169.6 mmol), LiCl (9.0 g, 212.1 mmol) and **6e** (15.0 g, 84.8 mmol) were added at rt. The mixture was stirred under reflux for 4.5 h. After cooling to rt, the product was collected by suction filtration, washed with EtOH (2 × 4.5 mL) and stirred with $H_2O$ (325 mL) for 1 h. The solids were collected by suction filtration, washed with $H_2O$ (2 × 11.5 mL) and dried at 50 °C under a gentle $N_2$ stream in a vacuum drying cabinet. Yield: 21.8 g (81%). $^1$H NMR (400 MHz, $CDCl_3$): δ = 8.51 (dd, *J* = 2.7, 1.7 Hz, 1H), 8.15 (dd, *J* = 7.7, 2.8 Hz, 1H), 7.19–7.33 (m, 1H), 6.93–7.16 (m, 3H), 5.88 (s, 2H), 4.52 (q, *J* = 7.2 Hz, 2H), 1.48 (t, *J* = 7.2 Hz, 3H). MS (ESI+): *m*/*z* = 318 $[M + H]^+$.

**5-Fluoro-1-(2-fluorobenzyl)-1*H*-pyrazolo[3,4-*b*]pyridine-3-carboxamide (6g).** EtOH (10 mL), formamide (14.9 mL, 441.2 mmol) and 30% NaOMe in MeOH (3.6 g, 19.8 mmol) were added to **6f** (7.0 g, 22.1 mmol). The reaction mixture was heated to 95–100 °C and the volatile solvents were distilled off by a downward distillation within 1h. The mixture was stirred at 125

°C for 1.5 h, $H_2O$ (30 mL) was added and the resulting mixture was cooled to rt and stirred for 1 h. The precipitated solids were collected by suction filtration, washed with $H_2O$ (3 × 8.5 mL) and dried at 45 °C under a gentle $N_2$ stream in a vacuum drying cabinet. Yield: 6.2 g (97%). $^1$H NMR (400 MHz, [$D_6$]DMSO): δ = 8.72 (dd, *J* = 2.7, 1.7 Hz, 1H), 8.28 (dd, *J* = 8.3, 2.8 Hz, 1H), 7.87 (br s, 1H), 7.60 (br s, 1H), 7.34–7.40 (m, 1H), 7.12–7.26 (m, 3H), 5.87 (s, 2H). MS (ESI+): *m*/*z* = 289 $[M + H]^+$.

**5-Fluoro-1-(2-fluorobenzyl)-1*H*-pyrazolo[3,4-*b*]pyridine-3-carbonitrile (6h). 6g** (17.3 g, 60.0 mmol) was heated to 103–107 °C in sulfolane (40.5 mL) and MeCN (5.4 mL). $POCl_3$ (6.9 g, 45.0 mmol) was slowly added dropwise while stirring, the dropping funnel was rinsed with MeCN (2.8 mL), and then the mixture was stirred at 107 °C for 1.5 h until conversion was complete (HPLC). Then, the mixture was cooled to rt and sulfolane/MeCN (5:1, 2.8 mL) and then $H_2O$ (17.8 mL) were added dropwise. The mixture was stirred for 0.5 h, a solution of aq $NH_3$ (28%, 9.4 g) in $H_2O$ (22.7 mL) was added dropwise and the resulting mixture was stirred for a further 2 h. The precipitated solids were collected by suction filtration, washed with $H_2O$ (3 × 20.5 mL) and dried at 50 °C under a gentle $N_2$ stream in a vacuum drying cabinet. Yield: 14.7 g (92%). $^1$H NMR (400 MHz, [$D_6$]DMSO): δ = 8.87 (dd, *J* = 2.6, 1.7 Hz, 1H), 8.52 (dd, *J* = 8.1, 2.6 Hz, 1H), 7.17–7.42 (m, 4H), 5.87 (s, 2H). MS (ESI+): *m*/*z* = 271 $[M + H]^+$.

**5-Fluoro-1-(2-fluorobenzyl)-1*H*-pyrazolo[3,4-*b*]pyridine-3-carboximidamide Hydrochloride (6i). 6h** (406.0 g, 1.50 mol) was suspended in EtOH (2.08 L). Then, 30% NaOMe in MeOH (54.1 g, 0.30 mol) was added and the mixture was stirred at rt overnight. $NH_4Cl$ (88.4 g, 1.65 mol) was added and the mixture was heated to 65 °C and stirred at 65 °C for 3.5 h. The solvents were distilled off and the residue was stirred with EtOAc (1.60 L) overnight. The precipitated

solids were collected by suction filtration, washed with EtOAc (2 × 140 mL) and dried at 50 °C under a gentle $N_2$ stream in a vacuum drying cabinet. Yield: 441.4 g (91%). $^1$H NMR (400 MHz, [$D_6$]DMSO): δ = 9.35 (br s, 3H), 8.86 (dd, *J* = 2.5, 1.5 Hz, 1H), 8.48 (dd, *J* = 8.8, 2.6 Hz, 1H), 7.36–7.43 (m, 1H), 7.29–7.35 (m, 1H), 7.22–7.28 (m, 1H), 7.15–7.20 (m, 1H), 5.90 (s, 2H). MS (ESI+): *m*/*z* = 288 $[M + H]^+$.

**2-[5-Fluoro-1-(2-fluorobenzyl)-1*H*-pyrazolo[3,4-*b*]pyridin-3-yl]-5-[(*E*)-phenyldiazenyl]pyrimidine-4,6-diamine (6j).** Concd HCl (262 g, 2.59 mol) and $H_2O$ (117.5 mL) were added dropwise at 0–5 °C to $H_2O$ (1.525 L) and aniline (117.5 g, 1.26 mol). Then, a solution of $NaNO_2$ (87.1 g, 1.26 mol) in $H_2O$ (222.5 mL) was added dropwise within 1 h, the dropping funnel was rinsed with $H_2O$ (60 mL), and the mixture was stirred at 0–5 °C for 15 min. Thereafter, at this temperature, a solution of NaOAc (131.4 g, 1.60 mol) in $H_2O$ (665 mL) was added dropwise within 45 min, the dropping funnel was rinsed with $H_2O$ (60 mL), and a solution of malononitrile (83.4 g, 1.26 mol) in EtOH (233 mL) was added dropwise within 1 h. The dropping funnel was rinsed with EtOH (68.5 mL) and the mixture was further stirred at 0–5 °C for 2 h. The yellow solids were collected by suction filtration and washed with $H_2O$ (3 × 625 mL) and cold toluene (488 mL). The still-moist residue was dissolved in DMF (872 g), which gave a DMF solution of [(*E*)-phenyldiazenyl]malononitrile (1.117 kg). **6i** (30.0 g, 92.7 mmol) was suspended in DMF (72 mL). The mixture was heated to 100 °C and a mixture of $Et_3N$ (14.2 mL, 101.9 mmol) and the DMF solution of [(*E*)-phenyldiazenyl]malononitrile (150 g) was added dropwise at this temperature within 30 min. The dropping funnel was rinsed with DMF (30 mL) and the mixture was further stirred at 100 °C for 20 h. Then, it was cooled to 95–90 °C, $H_2O$ (24 mL) was added dropwise within 10 min, and the resulting mixture was cooled to 0–5 °C within 1.5 h and stirred for 1 h. The solids were collected by suction filtration, washed with $H_2O$ (60

mL)/DMF (63 mL), twice with $H_2O$ (50 mL)/MeOH (63 mL) and then with MeOH (63 mL), suction-dried and then dried at 50 °C under a gentle $N_2$ stream in a vacuum drying cabinet. Yield: 35.5 g (84%). $^1$H NMR (400 MHz, [$D_6$]DMSO): δ = 9.03 (dd, *J* = 8.8, 2.8 Hz, 1H), 8.65–8.77 (m, 1H), 8.50 (br s, 2H), 8.02 (d, *J* = 7.6 Hz, 2H), 7.86–7.98 (m, 2H), 7.44–7.57 (m, 2H), 7.32–7.44 (m, 2H), 7.11–7.31 (m, 3H), 5.84 (s, 2H). LC-MS (method d): $^t$R (min) = 1.15. MS (ESI+): *m*/*z* = 458 $[M + H]^+$.

**2-[5-Fluoro-1-(2-fluorobenzyl)-1*H*-pyrazolo[3,4-*b*]pyridin-3-yl]pyrimidine-4,5,6-triamine (6k). 6j** (182.0 g, 0.39 mol) was initially charged into DMF (1.82 L) and then 5% Pd/C (50% water-moist, 4.2 g) was added. Hydrogenation was effected at 60 °C and $H_2$ pressure of 60 bar while stirring overnight. The mixture was filtered through kieselguhr and the solids were washed thoroughly with DMF (150 mL) and then with MeOH (150 mL). The filtrate was concentrated at 60–70 °C to a weight of 425 g of distillation residue. The residue was heated to 75–80 °C, MeOH (300 mL) was added dropwise at this temperature and the mixture was stirred for 15 min. The mixture was cooled to rt within 1 h, then $H_2O$ (1.29 L) was added dropwise and the mixture was stirred overnight. The solids were collected by suction filtration, washed with $H_2O$ (2 × 500 mL), suction-dried and then dried at 50 °C under a gentle $N_2$ stream in a vacuum drying cabinet. Yield: 159.7 g. For analytical purposes, a sample was purified by chromatography on silica gel (DCM/MeOH 9:1). $^1$H NMR (400 MHz, [$D_6$]DMSO): δ = 8.85 (dd, *J* = 9.0, 2.9 Hz, 1H), 8.62 (dd, *J* = 2.8, 1.7 Hz, 1H), 7.32–7.39 (m, 1H), 7.10–7.26 (m, 3H), 5.86 (br s, 4H), 5.75 (s, 2H), 4.04 (br s, 2H). MS (ESI+): *m*/*z* = 369 $[M + H]^+$.

**Methyl {4,6-Diamino-2-[1-(2-fluorobenzyl)-1*H*-pyrazolo[3,4-*c*]pyridazin-3-yl]pyrimidin-5-yl}carbamate Formic Acid Salt (21).** The crude intermediate (**3h**: 198 mg, 0.51 mmol) was

treated with pyridine (15.0 mL) and the mixture was cooled to 0 °C. Next, a solution of methyl chloroformate (43.6 μL, 0.57 mmol) in DCM (1.0 mL) was slowly added and the mixture was stirred at rt for 3 d. Additional methyl chloroformate (0.1 equiv) in DCM (1.0 mL) was added at 0 °C and the mixture was stirred for a further 30 min at rt. The reaction mixture was then concentrated and the residue was treated with MeCN. The resulting suspension was filtered and the filtrate was concentrated. The residue was purified by preparative reversed-phase HPLC ($H_2O$ + 0.05% formic acid/MeOH gradient) to give **21** as a white solid. Yield: 72 mg (33%, purity 97%). $^1$H NMR (400 MHz, [$D_6$]DMSO): δ = 9.28 (d, *J* = 5.4 Hz, 1H), 8.88 (d, *J* = 5.6 Hz, 1H), 8.15 (s, 1H), 7.95–8.06 (m, 1H), 7.34–7.43 (m, 1H), 7.12–7.33 (m, 4H), 6.17–6.32 (m, 4H), 6.01 (s, 2H), 3.62 (s, 3H). LC-MS (method d): $^t$R (min) = 0.66. MS (ESI+): *m*/*z* = 410 $[M + H]^+$.

**Methyl {4,6-Diamino-2-[8-(2-fluorobenzyl)imidazo[1,5-*a*]pyrimidin-6-yl]pyrimidin-5-yl}carbamate (22). 4j** (45 mg, 0.128 mmol) was dissolved in pyridine (3.46 mL) and the solution was cooled to 0 °C. Then, methyl chloroformate (12.9 μL, 0.167 mmol) was added and the mixture was stirred for an additional 5 min at 0 °C and for 19 h at rt. The resulting mixture was concentrated under reduced pressure to a volume of 1.5 mL and the residue was purified by preparative reversed-phase HPLC ($H_2O$ + 0.1% $NH_3$/MeCN gradient) to give **22** as a yellow solid. Yield: 24 mg (45%). $^1$H NMR (400 MHz, [$D_6$]DMSO): δ = 10.22 (d, *J* = 7.15 Hz, 1H), 8.28 (d, *J* = 3.8 Hz, 1H), 7.97 (br s, 0.65 H), 7.67 (br s, 0.35 H), 7.20–7.29 (m, 2H), 7.11–7.18 (m, 1H), 7.05–7.11 (m, 1H), 6.89 (dd, *J* = 3.7, 7.3 Hz, 1H), 6.24 (br s, 4H), 4.30 (s, 2H), 3.61 (br s, 3H). LC-MS (method d): $^t$R (min) = 0.73. MS (ESI+): *m*/*z* = 409 $[M + H]^+$.

**Methyl {4,6-Diamino-2-[5-fluoro-1-(2-fluorobenzyl)-1*H*-pyrazolo[3,4-*b*]pyridin-3-yl]pyrimidin-5-yl}carbamate (24). 6k** (77% by weight, 4.0 g, 8.36 mmol) in *i*-PrOH (37.9 mL)

was heated to 35 °C and then methyl chloroformate (0.84 mL, 10.87 mmol) was added dropwise. The mixture was stirred at 35–40 °C for 20 h, heated to 50 °C and MeOH (9.5 mL) was added. Then, $Et_3N$ (1.9 mL) was added dropwise within 0.5 h, the dropping funnel was rinsed with MeOH (1.3 mL) and the resulting mixture was stirred at 50 °C for 1 h. Thereafter, the mixture was cooled to rt and stirred at rt for 1 h. The solids were collected by suction filtration, washed with EtOH (3 × 8 mL), suction-dried and then dried at 50 °C under a gentle $N_2$ stream in a vacuum drying cabinet. Yield: 3.4 g of crude product. The crude product (3.0 g) was stirred in DMSO (8 mL) for 5 min, EtOAc (13.0 mL) and activated carbon (50 mg) were added and the mixture was heated under reflux (84 °C) for 15 min. The suspension was hot-filtered and the filter residue was washed with EtOAc (1.9 mL). EtOAc (60 mL) and EtOH (16 mL) were heated to 60 °C, the combined filtrates were added dropwise and the resulting mixture was stirred at 60 °C for 1.5 h. The suspension was cooled to rt within 25 min, stirred for a further 1.5 h, cooled further to 0–5 °C and stirred for a further 1 h. The solids were collected by suction filtration, washed with EtOAc (2 × 6.4 mL), suction-dried and then dried at 50 °C under a gentle $N_2$ stream in a vacuum drying cabinet to give **24**. Yield: 2.2 g (70%). $^1$H NMR (400 MHz, [$D_6$]DMSO): δ = 8.89 (dd, $J$ = 9.0, 2.8 Hz, 1H), 8.66 (m, 1H), 7.99 and 7.67 (2 br s, 1H), 7.32–7.40 (m, 1H), 7.19–7.26 (m, 1H), 7.10–7.19 (m, 2H), 6.22 (br s, 4H), 5.79 (s, 2H), 3.62 (br s, 3H). LC-MS (method d): $^t$R (min) = 0.79. MS (ESI+): $m/z$ = 427 $[M + H]^+$.

## Biology

**General.** Animal experiments were conducted in accordance with the German animal welfare laws, approved by local authorities and in accordance with the ethical guidelines of Bayer AG.

**CYP Inhibition Assay.** The inhibitory potency of **24** was assessed in vitro by means on formation of metabolites from standard probes mediated by CYP isoforms (for details please refer to the supporting information) based on assay conditions described.[50] To investigate time-dependent, pre-incubation experiments on CYP3A4 were performed.[51]

**In vitro Clearance Determinations with Rat and Human Hepatocytes.** Incubations with hepatocytes were performed at 37 °C, pH 7.4 in a total volume of 1.5 mL using a modified Janus robotic system (Perkin Elmer). The incubation mixtures contained $1 \cdot 10^6$ cells/mL (corrected, according to the viability of the cells, determined via microscopy after staining with trypan blue), 1 μM substrate and Williams' medium E (Sigma, Product No. W1878). The final MeCN concentration was ≤1%. Aliquots of 125 μL were withdrawn from the incubation mixture after 2, 10, 20, 30, 50, 70 and 90 min and dispensed in a 96-well plate, containing MeCN (250 μL) to stop the reaction. After centrifugation at 1000g, supernatants were analyzed by LC-MS/MS (AB Sciex Triple Quad 5500).

The calculation of in vitro clearance values from half-life data using hepatocytes, reflecting substrate depletion, was performed using the following equations: $CL'_{intrinsic}$ [mL/(min·kg)] = (0.693/in vitro $t_{1/2}$ [min]) (liver weight [g liver/kg body mass]) (cell no. [$1.1 \cdot 10^8$]/liver weight [g])/(cell no. [$1 \cdot 10^6$]/incubation volume [mL]). The $CL_{blood}$ was estimated using the nonrestricted well-stirred model: $CL_{blood}$ well-stirred [L/(h·kg)] = ($Q_H$ [L/(h·kg)]·$CL'_{intrinsic}$ [L/(h·kg)])/($Q_H$[L/(h·kg)] + $CL'_{intrinsic}$ [L/(h·kg)]). For calculations, the following values were used: human specific liver weight of 21 g/kg body mass, hepatic blood flow of 1.32 L/(h·kg), cell number in the liver was estimated to be $1.1 \cdot 10^8$ cells/g liver; rat specific liver weight of 32

g/kg body mass, hepatic blood flow of 4.2 L/(h·kg), cell number in the liver was estimated to be $1.1 \cdot 10^8$ cells/g liver.[52]

**Caco-2 Permeability Assay.** The in vitro permeation of test compounds across a Caco-2 cell monolayer, a well-established in vitro system to predict the permeability from the gastrointestinal tract, was tested according to Artursson and Karlsson.[53] Caco-2 cells (ACC 169, DSMZ, German Collection of Microorganisms and Cell Cultures, Braunschweig, Germany) were seeded on 24-well insert plates and were allowed to grow for 14 to 16 d. For permeability studies, the test compounds were dissolved in DMSO and diluted to the final test concentration of 2 μM with transport buffer [Hanks' buffered salt solution, Gibco/Invitrogen, further supplemented with glucose (final concentration 19.9 mM) and HEPES (final concentration 9.8 mM)]. For determination of the apical to basolateral permeability ($P_{app}$ A–B), the test compound solution was added to the apical side of the cell monolayer and transport buffer to the basolateral side of the monolayer. For determination of the basolateral to apical permeability ($P_{app}$ B–A), the test compound solution was added to the basolateral side of the cell monolayer and transport buffer to the apical side of the monolayer. Samples were taken from the donor compartment at the beginning of the experiment to confirm mass balance. After an incubation of 2 h at 37 °C, samples were taken from both compartments. Samples were analyzed by LC-MS and the apparent permeability coefficients were calculated. The efflux ratio was calculated as $P_{app}$ B–A/$P_{app}$ A–B. Lucifer yellow permeability was assayed for each cell monolayer to ensure cell monolayer integrity, and the permeability of atenolol (low permeability marker) and sulfasalazine (marker for active excretion) was determined for each batch as a quality control.

**Pharmacokinetic Parameters after Intravenous and Oral Application in Rats and Dogs.** For in vivo pharmacokinetic experiments, male Wistar rats and female beagle dogs were used.

Intravenous application was carried out with a species-specific plasma/DMSO formulation in rats and with a $H_2O$/PEG 400/EtOH formulation in dogs. Oral application in both species was by gavage with a $H_2O$/PEG 400/EtOH formulation. For simplification of blood drawing in rats, a silicone catheter was implanted into the right vena jugularis externa. The surgery was performed at least 1 d before substance application, under isoflurane anesthesia and additional administration of an analgetic (atropine/rimadyl 3:1, 0.1 mL sc). Blood drawing (usually more than 10 time points) was done in a time window that included at least two time points after 24 h (post-substance application). Blood was passed into heparinized tubes. Afterwards, blood plasma was obtained by centrifugation at 1000g. Where necessary, the plasma was stored at –20 °C until further analysis.

An internal standard was added to the sample, calibration and qualifier solutions. The internal standard could also have been a compound from a different chemical class than the analyte of interest. Afterwards, protein precipitation was performed by using an excess of MeCN. A buffer solution was added with a composition based on the mobile phases used in subsequent liquid chromatography. After centrifugation at 1000g, the supernatant was analyzed by LC-MS using different C18 reversed-phase columns and various mobile phase compositions. Quantification of the substance was conducted by using peak height or area calculated from extracted ion chromatograms of specific selected ion-monitoring experiments or high-resolution LC-MS experiments.

From the plasma concentration–time course, the pharmacokinetic parameters CL (clearance), $t_{1/2}$ (terminal half-life), $V_{SS}$ (volume of distribution at steady state) and $F$ (bioavailability after oral administration) were calculated by using a validated internal pharmacokinetic calculation software.

Since substance quantification was done in plasma, the blood/plasma distribution needed to be analyzed to calculate a blood clearance value. Therefore, a defined amount of the substance was added to blood in heparinized tubes and incubated for 20 min by gently swinging. The plasma was obtained by centrifugation at 1000g. The $c_{blood}/c_{plasma}$ value was calculated after measurement of the substance concentration in plasma and blood [by high resolution LC-MS/MS].

**Highly Purified sGC.** Enzyme activity was measured by the formation of [$^{32}$P]-cGMP from α-[$^{32}$P]-GTP, modified according to Hoenicka et al.[54] and Schermuly et al.[55] The modifications included using GTP, $Mn^{2+}/Mg^{2+}$ and cGMP at concentrations of 200 μM, 3 mM and 1 mM, respectively. Enzyme concentrations were chosen carefully to achieve a substrate turnover of less than 10%, thus avoiding substrate or cofactor depletion. The characterization of the purified enzyme was performed at a protein concentration of 0.2 μg/mL. All measurements were performed in duplicate and were repeated five times. For enzyme characterization, the specific activity of sGC was expressed as x-fold stimulation vs specific basal activity. The highest DMSO concentration in the assay was 1% (v/v) and did not elicit any effect per se on cGMP production.

**Recombinant sGC-Overexpressing Cell Line.** The cellular activity of the test compounds was determined using a recombinant sGC-overexpressing cell line, as previously described.[34] Briefly, cells were plated in a volume of 25 μL on white 384-well Greiner Bio-One microplates and were cultured for 1 or 2 d in medium. Medium was removed and cells were loaded for 3 h with calcium-free Tyrode-containing coelenterazine. Serial dilutions of the test compounds in a volume of 10 μL in calcium-free Tyrode were applied to the cells for 6 min. Thereafter, 35 μL

Tyrode-containing calcium (final concentration: 3 mM) was added to the cells and the emitted light was measured for 40 s using a CCD camera in a lighttight box. The minimal effective concentration (MEC) was determined as the concentration where a ≥3-fold increase in the basal luminescence value was observed.

**Isolated Vessels and Tolerance.** The relaxing effects of **24** on aortas, saphenous arteries, coronary arteries and veins, as well as the investigation on aortic rings taken from either normal or nitrate-tolerant rabbits, were performed as previously described.[39]

**Rat Heart Langendorff Preparation.** Male Wistar rats (200–250 g) were anesthetized using Narcoren (100 mg/kg ip). The heart was rapidly excised and connected to a Langendorff perfusion system (FMI GmbH, Seeheim-Ober Beerbach, Germany). The heart was perfused at a constant flow rate of 10 mL/min with Krebs-Henseleit buffer solution equilibrated with 95% $O_2$ and 5% $CO_2$. The perfusion solution contained (in mmol/L): NaCl 118, KCl 3, $NaHCO_3$ 22, $KH_2PO_4$ 1.2, $MgSO_4$ 1.2, $CaCl_2$ 1.8, glucose 10, sodium pyruvate 2. A pressure transducer registered the perfusion pressure in the system. The left ventricular pressure was measured using a second pressure transducer connected to a water-filled balloon which was inserted into the left ventricle via the left atrium. The end diastolic pressure was initially set to 8–10 mmHg by adjusting the volume of the balloon. The hearts were spontaneously beating. The signals from the pressure transducer were amplified, registered and used for the calculation of the heart frequency and $+dP/dt_{max}$ by a personal computer. **24** was dissolved in a mixture of 10% DMSO and 90% saline and infused for 20 min with increasing concentration steps into the aortic cannula at a rate of 1% of the total flow rate. All values are presented as relative changes of baseline values before compound application.

**Chronic Treatment Study with L-NAME-Treated Renin Transgenic Rats.** 50 male renin transgenic rats carrying an additional mouse renin gene [RenTG(mRRen2)27] at the age of 8 weeks were used. L-NAME was chronically administered via the drinking water (50 mg/L) in all study groups. Animals were randomly allocated to three study groups: placebo (control) (n = 20), **24** low dose and **24** high dose (3 and 10 mg/kg per day, respectively, administered po by gavage q.d., n = 15 per group). Blood pressure was measured via the tail-cuff method once before the start of the study (day 0) to exclude preexisting differences between the groups and on day 7, 14 and 21. Body weight and survival were assessed on day 1, 8 and 15, and at the study end. At the end of the study (day 22), all animals were anesthetized, blood was collected and animals were sacrificed; blood was taken in order to assess plasma parameters, and the heart was dissected into the left and right ventricles and was weighed to assess potential heart hypertrophy. Creatinine, urea and renin activity in plasma were determined after extraction, as previously described.[39, 56]

**Statistics.** The unpaired t-test was used to detect significant differences between the groups of interest. Results (mean ± SEM) were considered significant when the probability error (P) was less than 0.05, 0.01and 0.001 for *, **, and ***, respectively.

ASSOCIATED CONTENT

Supporting Information: $^{1}$H-NMR spectra of selected compounds **3**, **21**, **22**, and **24**. Table S6: CYP-inhibition results of **24**

## AUTHOR INFORMATION

**Corresponding Author**

* E-mail: markus.follmann@bayer.com

**Author Contributions**

The manuscript was written through contributions of all authors. All authors have given approval to the final version of the manuscript.

**Notes**

The authors declare the following competing financial interest(s): All authors are or have been employees of Bayer AG.

## ACKNOWLEDGMENTS

Picture used for abstract © DLR/taken from "Unseen Extremes: Mapping the World's Greatest Mountains" by courtesy of Deutsches Zentrum für Luft- und Raumfahrt e.V. (DLR).

## ABBREVIATIONS USED

sGC, soluble guanylate cyclase; cGMP, cyclic guanosine 5'-monophosphate; HMDS, hexamethyldisilazane; MEC, minimum effective concentration; clogD, calculated logarithm of distribution coefficient; $Cl_b$, blood clearance

## REFERENCES

(1) Evgenov, O. V.; Pacher, P.; Schmidt, P. M.; Hasko, G.; Schmidt, H. H. H. W.; Stasch, J.-P. NO-independent stimulators and activators of soluble guanylate cyclase: discovery and therapeutic potential. *Nat. Rev. Drug Discovery* **2006,** *5*, 755-768.

(2) Follmann, M.; Griebenow, N.; Hahn, M. G.; Hartung, I.; Mais, F.-J.; Mittendorf, J.; Schaefer, M.; Schirok, H.; Stasch, J.-P.; Stoll, F.; Straub, A. The chemistry and biology of soluble guanylate cyclase stimulators and activators. *Angew. Chem., Int. Ed.* **2013,** *52*, 9442-9462.

(3) Cerra, M. C.; Pellegrino, D. Cardiovascular cGMP-generating systems in physiological and pathological conditions. *Curr. Med. Chem.* **2007,** *14*, 585-599.

(4) Gladwin, M. T. Deconstructing endothelial dysfunction: soluble guanylyl cyclase oxidation and the NO resistance syndrome. *J. Clin. Invest.* **2006**, *116*, 2330–2332.

(5) Hoenicka, M.; Schmid, C. Cardiovascular effects of modulators of soluble guanylyl cyclase activity. *Cardiovasc. Hematol. Agents Med. Chem.* **2008**, *6*, 287–301.

(6) Priviero, F. B.; Webb, R. C. Heme-dependent and independent soluble guanylate cyclase activators and vasodilation. *J. Cardiovasc. Pharmacol.* **2010**, *56*, 229–233.

(7) Packer, C. S. Soluble guanylate cyclase (sGC) down-regulation by abnormal extracellular matrix proteins as a novel mechanism in vascular dysfunction: implications in metabolic syndrome. *Cardiovasc. Res.* **2006**, *69*, 302–303.

(8) Mayer, B.; Koesling, D. cGMP signalling beyond nitric oxide. *Trends Pharmacol. Sci.* **2001**, *22*, 546–548.

(9) Nioche, P.; Berka, V.; Vipond, J.; Minton, N.; Tsai, A. L.; Raman, C. S. Femtomolar sensitivity of a NO sensor from Clostridium botulinum. *Science* **2004**, *306*, 1550–1553.

(10) Pellicena, P.; Karow, D. S.; Boon, E. M.; Marletta, M. A.; Kuriyan, J. Crystal structure of an oxygen-binding heme domain related to soluble guanylate cyclases. *Proc. Natl. Acad. Sci. U. S. A.* **2004**, *101*, 12854–12859.

(11) Wedel, B.; Humbert, P.; Harteneck, C.; Foerster, J.; Malkewitz, J.; Bohme, E.; Schultz, G.; Koesling, D. Mutation of His-105 in the $\beta_1$ subunit yields a nitric oxide-insensitive form of soluble guanylyl cyclase. *Proc. Natl. Acad. Sci. U. S. A.* **1994,** *91*, 2592-2596.

(12) Zabel, U.; Hausler, C.; Weeger, M.; Schmidt, H. H. Homodimerization of soluble guanylyl cyclase subunits. Dimerization analysis using a glutathione *S*-transferase affinity tag. *J. Biol. Chem.* **1999,** *274*, 18149-18152.

(13) Zabel, U.; Weeger, M.; La, M.; Schmidt, H. H. Human soluble guanylate cyclase: functional expression and revised isoenzyme family. *Biochem. J.* **1998,** *335 ( Pt 1)*, 51-57.

(14) Murad, F. Shattuck Lecture. Nitric oxide and cyclic GMP in cell signaling and drug development. *N. Engl. J. Med.* **2006,** *355*, 2003-2011.

(15) Stasch, J. P.; Hobbs, A. J. NO-independent, haem-dependent soluble guanylate cyclase stimulators. *Handb. Exp. Pharmacol.* **2009**, *191,* 277-308.

(16) Schmidt, H. H.; Schmidt, P. M.; Stasch, J. P. NO- and haem-independent soluble guanylate cyclase activators. *Handb. Exp. Pharmacol.* **2009**, *191*, 309-339.

(17) Stasch, J.-P.; Evgenov, O. V. Soluble guanylate cyclase stimulators in pulmonary hypertension. *Handb. Exp. Pharmacol.* **2013**, *218*, 279–313.

(18) Ghofrani, H.-A.; Galie, N.; Grimminger, F.; Gruenig, E.; Humbert, M.; Jing, Z.-C.; Keogh, A. M.; Langleben, D.; Kilama, M. O.; Fritsch, A.; Neuser, D.; Rubin, L. J. Riociguat for the treatment of pulmonary arterial hypertension. *N. Engl. J. Med.* **2013**, *369*, 330–340.

(19) Ghofrani, H.-A.; D'Armini, A. M.; Grimminger, F.; Hoeper, M. M.; Jansa, P.; Kim, N. H.; Mayer, E.; Simonneau, G.; Wilkins, M. R.; Fritsch, A.; Neuser, D.; Weimann, G.; Wang, C. Riociguat for the treatment of chronic thromboembolic pulmonary hypertension. *N. Engl. J. Med.* **2013**, *369*, 319–329.

(20) Hambly, N.; Granton, J. Riociguat for the treatment of pulmonary hypertension. *Expert Rev. Respir. Med.* **2015**, *9*, 679–695.

(21) Frey, R.; Mueck, W.; Unger, S.; Artmeier-Brandt, U.; Weimann, G.; Wensing, G. Single-dose pharmacokinetics, pharmacodynamics, tolerability, and safety of the soluble guanylate cyclase stimulator BAY 63-2521: an ascending-dose study in healthy male volunteers. *J. Clin. Pharmacol.* **2008**, *48*, 926–934.

(22) Gheorghiade, M.; Greene, S. J.; Butler, J.; Filippatos, G.; Lam, C. S.; Maggioni, A. P.; Ponikowski, P.; Shah, S. J.; Solomon, S. D.; Kraigher-Krainer, E.; Samano, E. T.; Müller, K.; Roessig, L.; Pieske, B. Effect of vericiguat, a soluble guanylate cyclase stimulator, on natriuretic peptide levels in patients with worsening chronic heart failure and reduced ejection fraction: the SOCRATES-REDUCED randomized trial. *JAMA, J. Am. Med. Assoc.* **2015**, *314*, 2251–2262.

(23) Pieske, B.; Butler, J.; Filippatos, G.; Lam, C.; Maggioni, A. P.; Ponikowski, P.; Shah, S.; Solomon, S.; Kraigher-Krainer, E.; Samano, E. T.; Scalise, A. V.; Mueller, K.; Roessig, L.; Gheorghiade, M. Rationale and design of the SOluble guanylate Cyclase stimulatoR in heArT failurE Studies (SOCRATES). *Eur. J. Heart Failure* **2014,** *16*, 1026-38.

(24) Clinicaltrials.gov. Identifier: NCT02861534 (accessed August 5, **2016**).

(25) Mittendorf, J.; Weigand, S.; Alonso-Alija, C.; Bischoff, E.; Feurer, A.; Gerisch, M.; Kern, A.; Knorr, A.; Lang, D.; Muenter, K.; Radtke, M.; Schirok, H.; Schlemmer, K.-H.; Stahl, E.; Straub, A.; Wunder, F.; Stasch, J.-P. Discovery of riociguat (BAY 63-2521): a potent, oral stimulator of soluble guanylate cyclase for the treatment of pulmonary hypertension. *ChemMedChem* **2009**, *4*, 853–865.

(26) Gnoth, M. J.; Hopfe, P. M.; Czembor, W. Determination of riociguat and its major human metabolite M-1 in human plasma by stable-isotope dilution LCMS/MS. *Bioanalysis* **2015**, *7*, 193–205.

(27) Becker, C.; Frey, R.; Thomas, D.; Reber, M.; Weimann, G.; Arens, E. R.; Muck, W.; Unger, S.; Dietrich, H. Pharmacokinetic interaction of riociguat with ketoconazole, clarithromycin, and midazolam. *Pulm. Circ.* **2016**, *6*, S49–57.

(28) Frey, R.; Becker, C.; Unger, S.; Schmidt, A.; Wensing, G.; Muck, W. Assessment of the effects of renal impairment and smoking on the pharmacokinetics of a single oral dose of the soluble guanylate cyclase stimulator riociguat (BAY 63-2521). *Pulm. Circ.* **2016**, *6*, S15–26.

(29) Saleh, S.; Frey, R.; Becker, C.; Unger, S.; Wensing, G.; Muck, W. Bioavailability, pharmacokinetics, and safety of riociguat given as an oral suspension or crushed tablet with and without food. *Pulm. Circ.* **2016**, *6*, S66–74.

(30) Zhao, X.; Wang, Z.; Wang, Y.; Zhang, H.; Blode, H.; Yoshikawa, K.; Becker, C.; Unger, S.; Frey, R.; Cui, Y. Pharmacokinetics of the soluble guanylate cyclase stimulator riociguat in healthy young Chinese male non-smokers and smokers: results of a randomized, double-blind, placebo-controlled study. *Clin. Pharmacokinet.* **2016**, *55*, 615–624.

(31) FDA. Highlights of prescribing information: riociguat (Adempas). **2014**, http://www.accessdata.fda.gov/drugsatfda_docs/label/2014/204819s002lbl.pdf, (accessed April 4, **2014**).

(32) Bitterli, P.; Erlenmeyer, H. Some derivatives of triazolopyrimidine. *Helv. Chim. Acta* **1951,** 34, 835-840.

(33) Reinecke, M. G.; Woodrow, T. A.; Brown, E. S. Pyrazolo[3,4-*c*]pyridazines from hydrazine and aminothiophenecarboxylates. *J. Org. Chem.* **1992**, *57*, 1018–1021.

(34) Wunder, F.; Stasch, J.-P.; Hütter, J.; Alonso-Alija, C.; Hüser, J.; Lohrmann, E. A cell-based cGMP assay useful for ultra-high-throughput screening and identification of modulators of the nitric oxide/cGMP pathway. *Anal. Biochem.* **2005**, *339*, 104–112.

(35) Hillisch, A.; Heinrich, N.; Wild, H. Computational chemistry in the pharmaceutical industry: from childhood to adolescence. *ChemMedChem* **2015**, *10*, 1958–1962.

(36) Burkhard, J. A.; Wuitschik, G.; Rogers-Evans, M.; Müller, K.; Carreira, E. M. Oxetanes as versatile elements in drug discovery and synthesis. *Angew. Chem. Int. Ed.* **2010**, *49*, 9052–9067.

(37) Wuitschik, G.; Carreira, E. M.; Wagner, B.; Fischer, H.; Parrilla, I.; Schuler, F.; Rogers-Evans, M.; Müller, K. Oxetanes in drug discovery: structural and synthetic insights. *J. Med. Chem.* **2010**, *53*, 3227–3246.

(38) Leeson, P. D.; Young, R. J. Molecular property design: does everyone get it? *ACS Med. Chem. Lett.* **2015**, *6*, 722-725.

(39) Sharkovska, Y.; Kalk, P.; Lawrenz, B.; Godes, M.; Hoffmann, L. S.; Wellkisch, K.; Geschka, S.; Relle, K.; Hocher, B.; Stasch, J.-P. Nitric oxide-independent stimulation of soluble guanylate cyclase reduces organ damage in experimental low-renin and high-renin models. *J. Hypertens.* **2010**, *28*, 1666–1675.

(40) Dubin, R. F.; Shah, S. J. Soluble guanylate cyclase stimulators: a novel treatment option for heart failure associated with cardiorenal syndromes? *Curr. Heart Failure Rep.* **2016**, *13*, 132–139.

(41) Follmann, M.; Stasch, J.-P.; Redlich, G.; Griebenow, N.; Lang, D.; Wunder, F.; Huebsch, W.; Lindner, N.; Vakalopoulos, A.; Tersteegen, A. Preparation of annelated pyrimidine

derivatives useful in the treatment and prophylaxis of cardiovascular diseases. WO2013030288, 2013.

(42) Follmann, M.; Stasch, J.-P.; Redlich, G.; Ackerstaff, J.; Griebenow, N.; Knorr, A.; Wunder, F.; Li, V. M.-J.; Baerfacker, L.; Weigand, S. Bicyclic aza-heterocycles as guanylate cyclase inhibitors and their preparation and use in the treatment of cardiovascular diseases. WO 2012028647, 2012.

(43) Follmann, M.; Stasch, J.-P.; Redlich, G.; Ackerstaff, J.; Griebenow, N.; Knorr, A.; Wunder, F.; Li, V. M.-J.; Schirok, H.; Jautelat, R. Substituted methyl pyrimidin-5-yl carbamates as guanylate cyclase inhibitors and their preparation and use in the treatment of cardiovascular diseases. WO 2012010578, 2012.

(44) Alonso-Alija, C.; Bischoff, E.; Muenter, K.; Stasch, J.-P.; Stahl, E.; Weigand, S.; Feurer, A. Preparation of [(pyrazolopyridinyl)pyrimidinyl]carbamates stimulating soluble guanylate cyclase for treating cardiovascular diseases and/or sexual dysfunction. WO 2003095451, 2003.

(45) Follmann, M.; Stasch, J.-P.; Redlich, G.; Ackerstaff, J.; Griebenow, N.; Wunder, F.; Li, V. M.-J.; Mittendorf, J.; Jautelat, R. Carbamate-substituted diaminopyrimidines as guanylate cyclase inhibitors and their preparation and use in the treatment of cardiovascular diseases. WO 2012010576, 2012.

(46) Schirok, H.; Mittendorf, J.; Stasch, J.-P.; Wunder, F.; Stoll, F.; Schlemmer, K.-H. Azabicyclic derivatives as stimulators of guanylate cyclase, their preparation, pharmaceutical compositions, and use for the treatment of cardiovascular disorders. WO 2008031513, 2008.

(47) Follmann, M.; Stasch, J.-P.; Redlich, G.; Ackerstaff, J.; Griebenow, N.; Knorr, A.; Wunder, F.; Li, V. M.-J.; Mittendorf, J.; Schlemmer, K.-H.; Jautelat, R. Substituted 6-fluoro-1*H*-pyrazolo[4,3-*b*]pyridines as guanylate cyclase inhibitors and their preparation and use in the treatment of cardiovascular diseases. WO 2012059549, 2012.

(48) Follmann, M.; Stasch, J.-P.; Redlich, G.; Straub, A.; Ackerstaff, J.; Griebenow, N.; Knorr, A.; Wunder, F.; Li, V. M.-J. Substituted imidazopyridazines as guanylate cyclase inhibitors and their preparation and use in the treatment of cardiovascular diseases. WO 2012152630, 2012.

(49) Straub, A.; Feurer, A.; Alonso-Alija, C.; Stasch, J.-P.; Perzborn, E.; Huetter, J.; Dembowsky, K.; Stahl, E. Substituted pyrazole derivatives condensed with six-membered heterocyclic rings as cardiovascular agents and their preparation. WO 2000006569, 2000.

(50) Walsky, R. L.; Obach, R. S. Validated assays for human cytochrome P450 activities. *Drug Metab. Dispos.* **2004**, *32*, 647-660.

(51) Obach, R. S.; Walsky, R. L.; Venkatakrishnan, K. Mechanism-based inactivation of human cytochrome p450 enzymes and the prediction of drug-drug interactions. *Drug Metab. Dispos.* **2007**, *35*, 246-255.

(52) Obach, R. S. Predicting clearance in humans from in vitro data. *Curr. Top. Med. Chem.* **2011**, *11*, 334-339.

(53) Artursson, P.; Karlsson, J. Correlation between oral drug absorption in humans and apparent drug permeability coefficients in human intestinal epithelial (Caco-2) cells. *Biochem. Biophys. Res. Commun.* **1991**, *175*, 880–885.

(54) Hoenicka, M.; Becker, E.-M.; Apeler, H.; Sirichoke, T.; Schröder, H.; Gerzer, R.; Stasch, J.-P. Purified soluble guanylyl cyclase expressed in a baculovirus/Sf9 system: stimulation by YC-1, nitric oxide, and carbon monoxide. *J. Mol. Med. (Heidelberg, Ger.)* **1999**, *77*, 14–23.

(55) Schermuly, R. T.; Stasch, J.-P.; Pullamsetti, S. S.; Middendorff, R.; Müller, D.; Schlüter, K.-D.; Dingendorf, A.; Hackemack, S.; Kolosionek, E.; Kaulen, C.; Dumitrascu, R.; Weissmann, N.; Mittendorf, J.; Klepetko, W.; Seeger, W.; Ghofrani, H. A.; Grimminger, F. Expression and function of soluble guanylate cyclase in pulmonary arterial hypertension. *Eur. Respir. J.* **2008**, *32*, 881–891.

(56) Geschka, S.; Kretschmer, A.; Sharkovska, Y.; Evgenov, O. V.; Lawrenz, B.; Hucke, A.; Hocher, B.; Stasch, J.-P. Soluble guanylate cyclase stimulation prevents fibrotic tissue remodeling and improves survival in salt-sensitive Dahl rats. *PLoS One* **2011**, *6*, e21853.

Table of contents graphic:

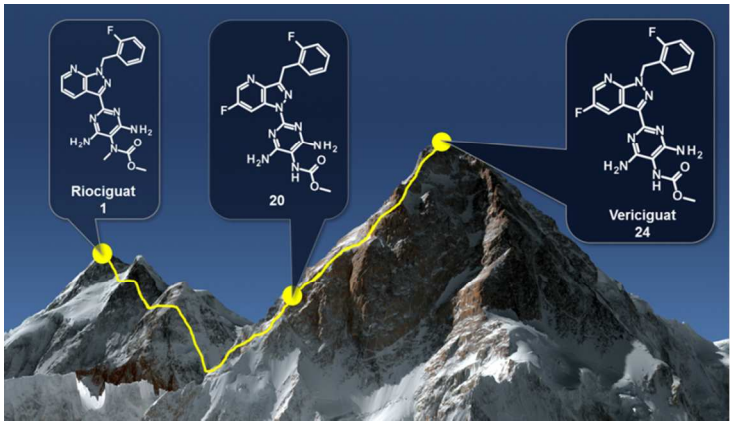

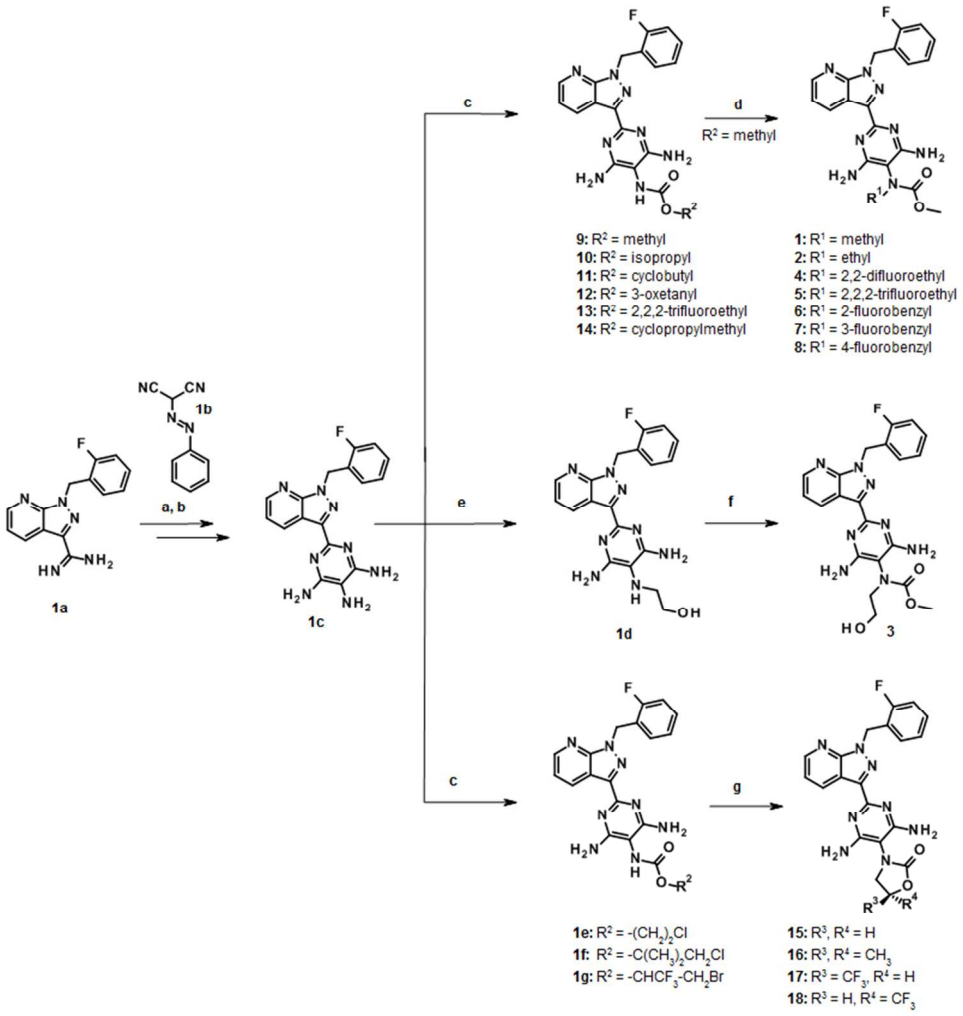


Synthesis of Compounds 1–18

221x223mm (96 x 96 DPI)

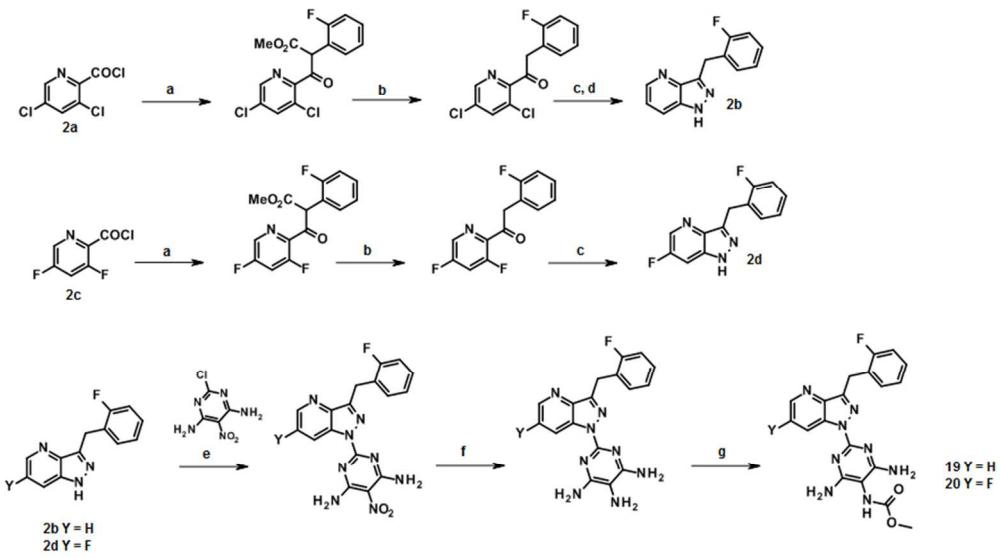


Synthesis of Compounds 19 and 20

233x129mm (96 x 96 DPI)

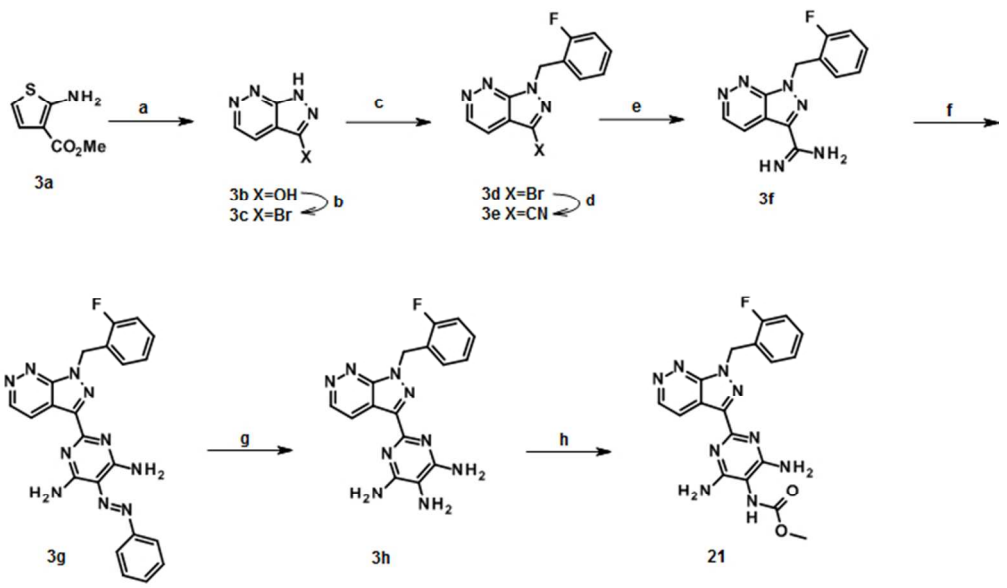


Synthesis of Compound 21

190x112mm (96 x 96 DPI)

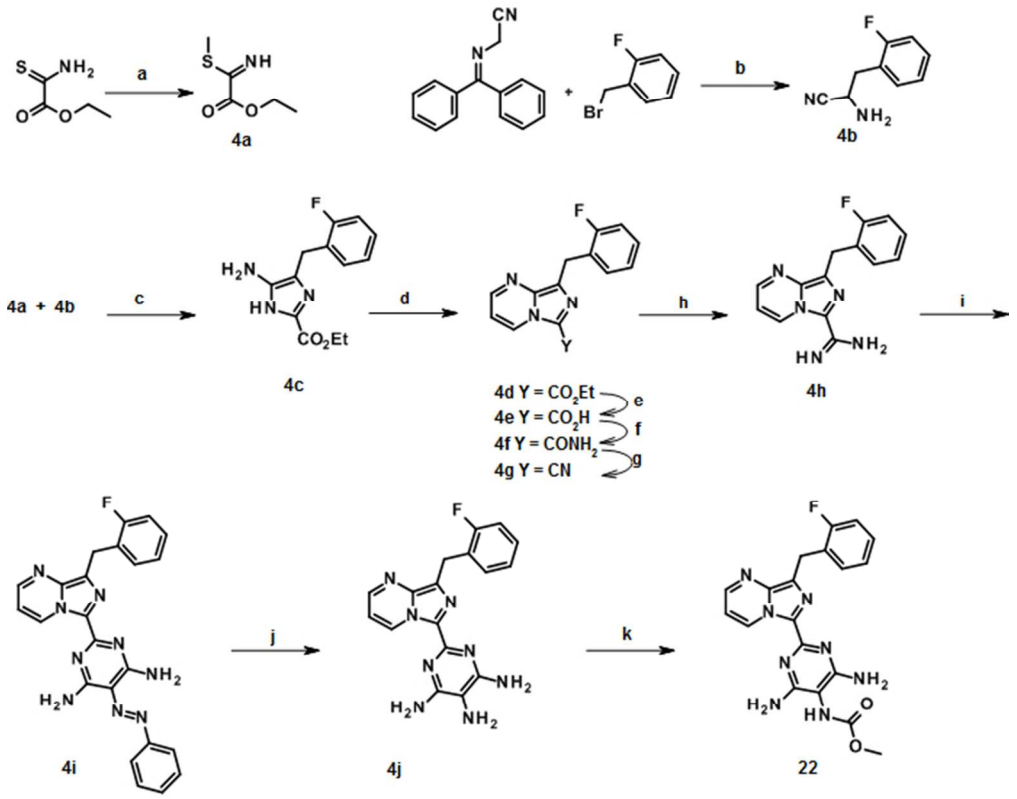


Synthesis of Compound 22

182x146mm (96 x 96 DPI)

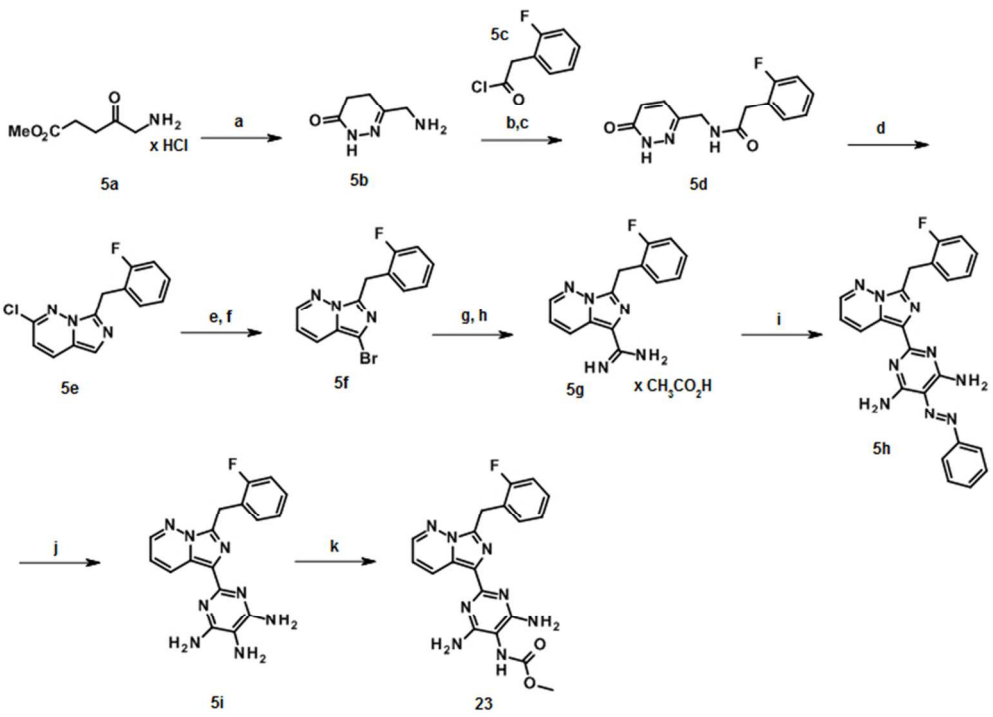


Synthesis of Compound 23

199x142mm (96 x 96 DPI)

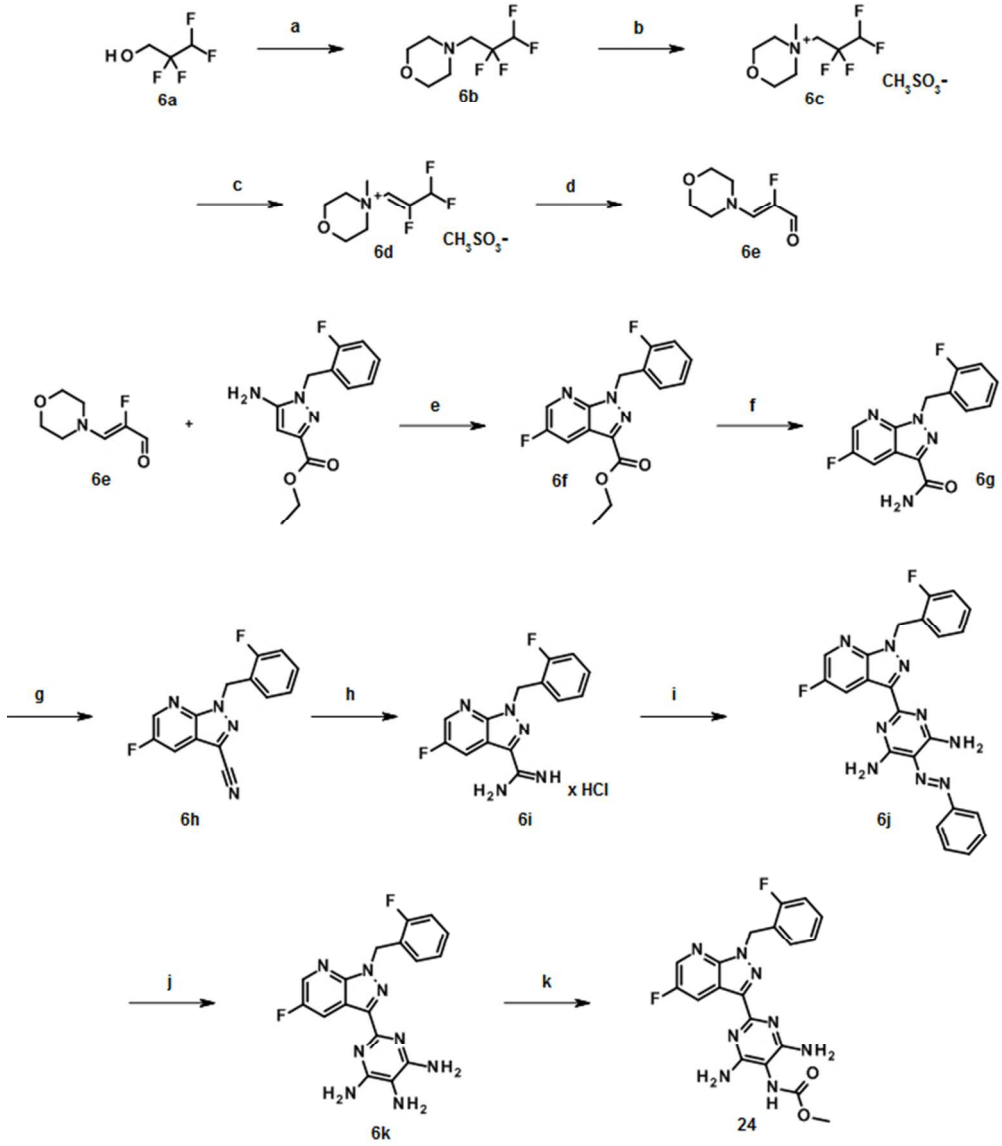


Synthesis of Vericiguat (24)

187x215mm (96 x 96 DPI)

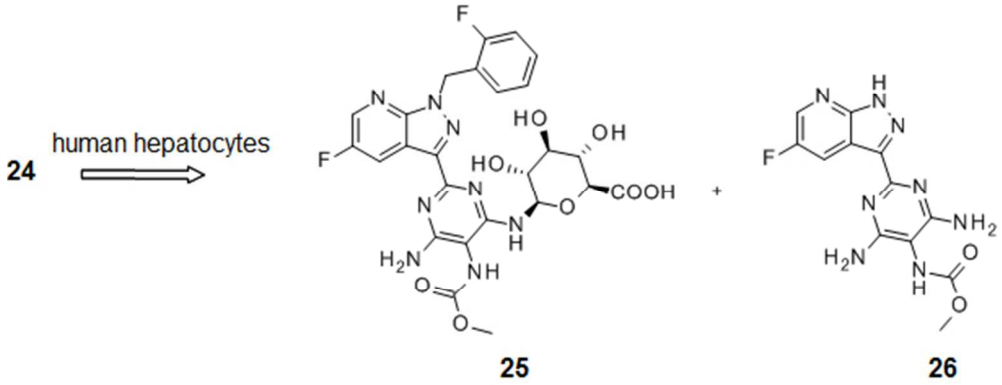


Figure 1. Biotransformation products of vericiguat (24) in human hepatocytes.

162x63mm (96 x 96 DPI)

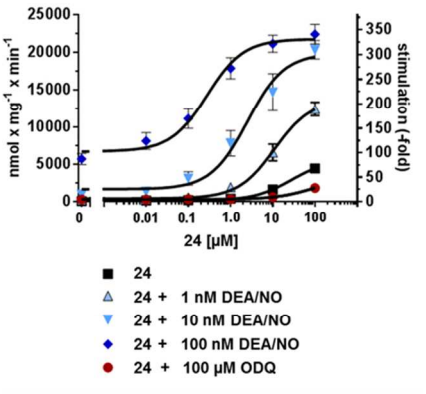


Figure 2. Effects of 24 and NO on the stimulation of highly purified sGC, and blocking effects of the sGC inhibitor ODQ.

266x166mm (96 x 96 DPI)

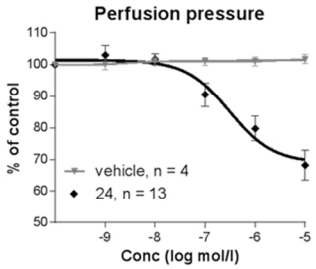


Figure 3. Effects of 24 on rat heart Langendorff preparations.

266x166mm (96 x 96 DPI)

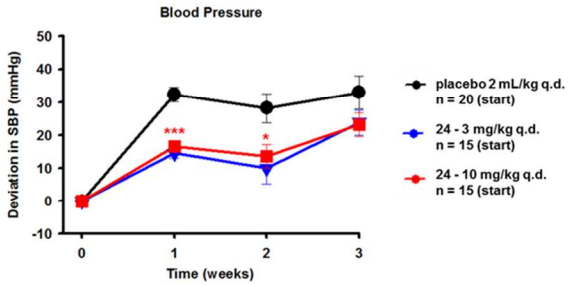


Figure 4. Increase in systolic blood pressure in mmHg during the course of the study with L-NAME-treated renin transgenic rats.

266x166mm (96 x 96 DPI)

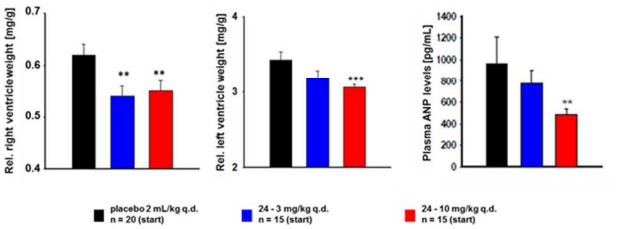


Figure 5. Right and left ventricle weight normalized on body weight (left/middle) and plasma atrial natriuretic peptide levels [in pg/mL] at the study end, after 3 weeks of treatment.

266x166mm (96 x 96 DPI)

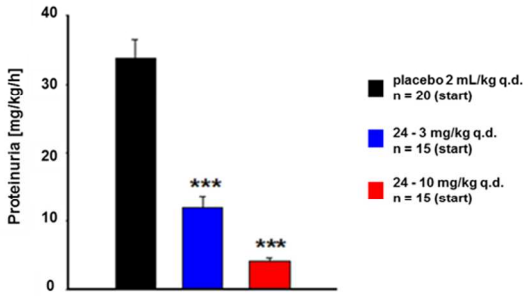


Figure 6. Effects on proteinuria at the study end, after 3 weeks of treatment.

266x166mm (96 x 96 DPI)

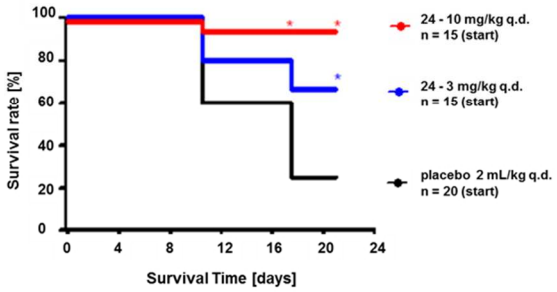


Figure 7. Kaplan–Meier survival curves.

266x166mm (96 x 96 DPI)

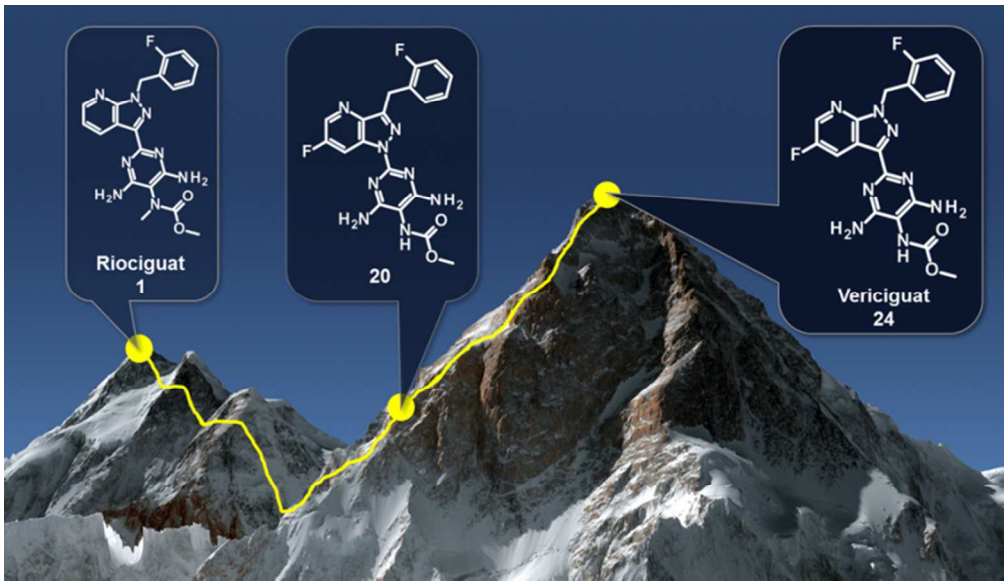


95x55mm (220 x 220 DPI)